THE UNIVERSITY OF MICHIGAN
COLLEGE OF ENGINEERING
Department of Mechanical Engineering

Semiannual Report

USE OF ACOUSTIC EMISSION IN NONDESTRUCTIVE TESTING

March 1, 1969 - August 31, 1969

J. R. Frederick

ORA Project 01971

under contract with:

UNITED STATES AIR FORCE
AIR FORCE SYSTEMS COMMAND
AERONAUTICAL SYSTEMS DIVISION
CONTRACT NO. F33615-68-C-1703
WRIGHT PATTERSON AIR FORCE BASE, OHIO

ARPA Order No. 1244
Program Code No. 8D10

administered through:

OFFICE OF RESEARCH ADMINISTRATION ANN ARBOR

November 1969

ABSTRACT

Acoustic emission may be defined as the noise given off spontaneously by solid materials as a result of a sudden relaxation of stresses within the material. Stress relaxation can occur as a result of the nucleation or propagation of cracks, or as a consequence of various elastic or plastic deformation processes. The principal elastic or plastic deformation mechanisms that are sources of acoustic emission in solids are: (1) the slip of existing dislocation in a metal, (2) the activation of dislocation sources, (3) twinning, and (4) grain boundary slip. This report describes the results of an investigation into the effects of the microstructure on acoustic emission. The characteristics of the emission that is observed in some materials when the load is removed from a specimen are described, and an explanation of this phenomenon on the basis of dislocation motion is given.

FOREWORD

This is the second semiannual report on a study of the use of acoustic emission in nondestructive testing. This research is supported by the Advanced Research Project Agency of the Department of Defense and is monitored by the Air Force Materials Laboratory, MANN, under Contract No. F33615-68-C-1703, initiated under ARPA Order 1244, Program Code 8D10. Mr. R. R. Rowand (MANN) is project engineer. This report covers the period from July 1, 1968 to August 31, 1969.

The program is being carried out in the Rheology and Fracture Laboratories of the Mechanical Engineering Department at The University of Michigan. The work is under the direction of Associate Professor J. R. Frederick. Professor David K. Felbeck, Dr. A. Agarwall, Mr. Robert Bill, Mr. G. Sankar, Mr. Charles Thomas, and Mr. M. Shah have participated in the program.

LIST OF FIGURES

Figure		Page
1.	Schematic of the acoustic tensile testing machine	4
2.	Schematic of the acoustic emission instrumentation system	6
3.	Acoustic emission test specimen	7
4.	Acoustic emission from a 99.99% aluminum alloy specimen at two different stresses	9
5.	Stress vs cumulative load emission, unload emission, and cumulative plastic strain in an annealed 99.99% aluminum specimen	10
6.	Effect of the grain size on the unload emission of 99.99% aluminum specimens. (a) Acoustic emission from a specimen of average grain size of 125 microns. (b) Acoustic emission from a specimen of average grain size of 15 microns, at two different stresses	11
7.	Effect of the grain size on the unload emission of 99.99% aluminum	13
8.	Stress vs cumulative load emission, unload emission and cumulative plastic strain in an annealed 6061 aluminum alloy specimen	14
9.	Stress vs cumulative load emission, unload emission in an annealed 2024 aluminum alloy specimen	15
10.	Aging time vs unload emission and hardness for 6061 aluminum alloy specimens	17
11.	Stress vs cumulative load emission, unload emission and cumulative plastic strain in an annealed copper-7.9% aluminum alloy	20
12.	Load emission in second loading vs unload emission in certain annealed materials	21
13.	Acoustic emission from annealed 99.95% magnesium	22
14.	Stress vs cumulative load emission, unload emission and cumulative plastic strain in annealed 70-30 brass	24
15.	Method for calculating the Bauschinger strain from the tension-compression load test data	25
16.	Bauschinger effect in several annealed materials	27
17.	Bauschinger effect in 2024 aluminum alloy specimens heat treated to produce different microstructures	28

LIST OF FIGURES (CONT'D)

Figure Page

18. Reverse plastic flow on unloading..... 30

19. Strain vs unload emission for several annealed materials..... 38

LIST OF TABLES

Table		Page
I	Compositions of the Materials Used	5
II	Aging Time and Resultant Hardness of 6061 Aluminum Alloy	16
III	Age Hardening Treatment, Hardness and the Resultant Microstructure in 2024 Aluminum Alloy	18
IV	Bauschinger Effect and Unload Emission in 2024 Aluminum Alloy, Heat Treated to Give Different Microstructures	42
V	Stacking Fault Energy, Bauschinger Effect and Unload Emission in Several Annealed Materials	46

1.0 Summary

Materials exhibit considerable acoustic emission when loaded in tension, and have been observed to also show emission when a tensile load is removed. The purpose of the work being reported here was to study the load and unload emission behavior of certain materials with various heat-treatments and to determine if a correlation exists between the Bauschinger effect and the acoustic emission observed during the removal of a load.

The materials tested were 99.99% aluminum, 6061 and 2024 aluminum alloys, copper-7.9% aluminum alloy, 70-30 brass and 99.95% magnesium.

The unload emission from all the materials tested was of the burst type. When the applied stress was increased, the unload emission increased, reached a peak value and then decreased. Among the fcc materials tested, 99.99% aluminum showed the least unload emission and copper-7.9% aluminum alloy the largest unload emission for the same plastic strain. A 99.95% magnesium showed even higher unload emission than a copper-7.9% aluminum alloy. Of the fcc materials tested, the copper-7.9% aluminum and 70-30 brass showed significant acoustic emission on repeated loading, thus indicating that a "Kaiser" effect is not always present.

Bauschinger tests were conducted on materials having the same chemical composition as those used in the acoustic emission study. Copper-7.9% aluminum alloy showed a large Bauschinger effect and 99.99% aluminum showed the least effect.

The following conclusions are drawn from the test results.

Unload emission is the result of reverse plastic deformation. Materials with high stacking fault energies, such as 99.99% aluminum,

give low acoustic emission during unloading. This is due to an increasing tendency for cross-slipping in such materials. On the other hand, planar glide materials, such as copper-7.9% aluminum alloy, with low stacking fault energy, show considerable acoustic emission during unloading. The unload emission in large grain size samples is larger, if other conditions remain the same.

Materials that show large acoustic emission during unloading show acoustic emission during repeated loading, even before reaching the maximum stress level of the first loading. It is likely that the dislocations are confined to primary slip planes and, hence, can move back and forth during unloading and repeated loading.

There is a good correlation between the Bauschinger effect and the unload emission. Materials that show a large Bauschinger effect show a large unload emission.

2.0 Objectives of the Program

The objectives of the work being reported in this contract period have been: (1) to determine the effect of microstructure on the load and unload acoustic emission from metals, and (2) to verify a model for unload emission that is based on the Bauschinger effect.

3.0 Experimental Procedure

Because of low level of the acoustic emission phenomena being studied and the frequency bands being used, a low-noise level loading system that has been previously described has been used[1]. Schematic diagrams of the mechanical components and the instrumentation are shown in Figs. 1 and 2.

The load is applied to the specimen by float and lever system shown in Fig. 1. This is located inside an audiometric room which has a noise reduction capability of 60 db for an octave band of 4800-9600 Hz. The low noise level preamplifier is also located inside the audiometric chamber and adjacent to the test specimen so that the input lead to it is short.

The materials tested were 99.99% aluminum supplied by the Aluminum Company of America, 2024 and 6061 aluminum alloys, copper-7.9% aluminum alloy, and 70-30 brass. All these materials are of fcc structure. Tests were also conducted on high purity magnesium (99.95%), an hcp material. All the samples were polycrystalline. The compositions of the various materials tested are shown in Table I.

Specimens were machined to the shape and size shown in Fig. 3 in order to produce yielding in the test section without an applied load in excess of 1000 lb.

A standard 50,000 lb testing machine, Model FGT made by Baldwin Lima Hamilton Corporation, was used to determine the magnitude of the Bauschinger effect for the various materials. This machine had grips that allowed tensile and compressive loads to be conveniently applied to the specimen.

4.0 Experimental Results

4.1 Acoustic Emission Behavior of 99.99% Aluminum

Aluminum bars of 1 in. diameter and 99.99% purity were obtained from the Aluminum Company of America. The bars were rolled to about 1/8 in. thickness and standard test specimens, as shown in Fig. 3, were machined from the sheet. The specimens were annealed at 970°F for 3 hours.

* indicates that acoustic isolation or mismatch material is used.

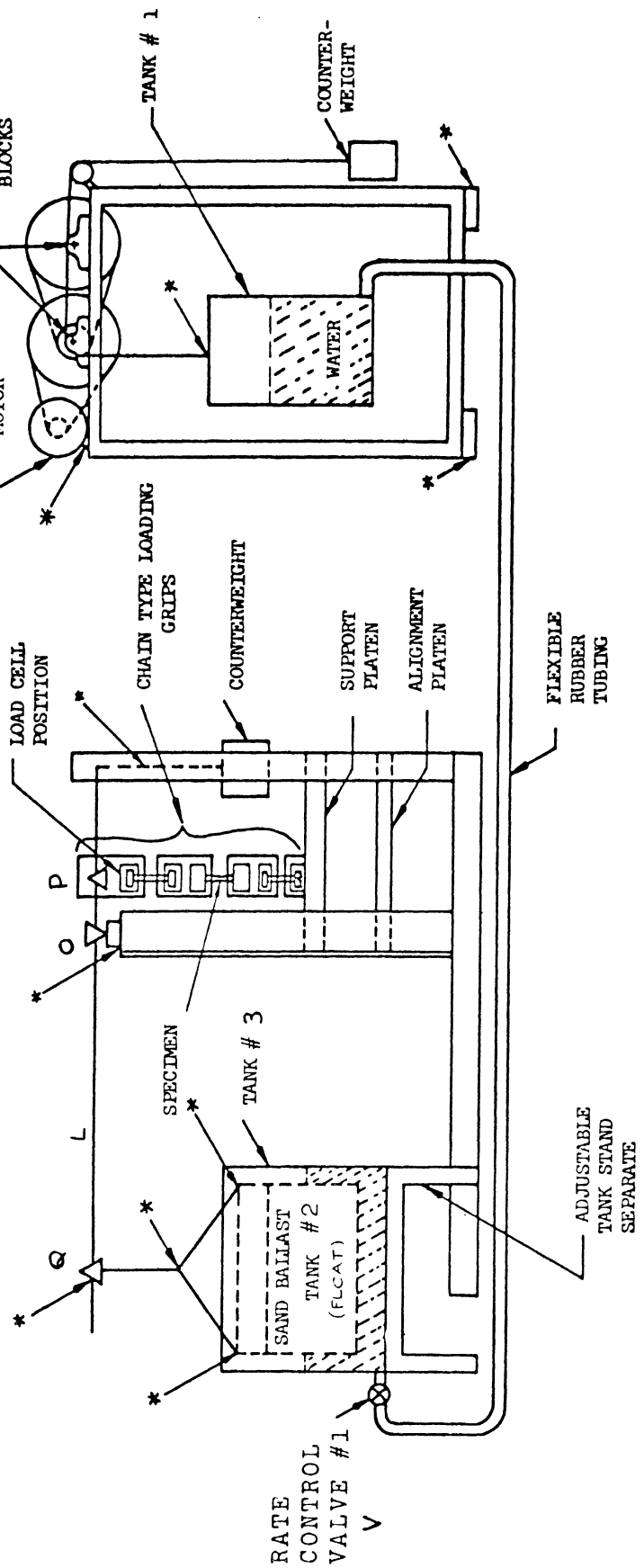

Figure 1 Schematic of the Acoustic Tensile Testing Machine.

TABLE I

COMPOSITIONS OF THE MATERIALS USED

(a) Aluminum and aluminum alloys

Type	Cu	Fe	Si	V	Zn	Mn	Mg	Cr	Al
99.99%	0.003	0.004	0.001	0.001	0.001	---	---	---	bal
6061 alloy	0.25	---	0.6	---	---	---	1.0	0.25	bal
2024 alloy	4.5	---	---	---	---	0.6	1.5	---	bal

(b) Magnesium*

Type	Al	Fe	Mn	Ni	Si	Ca	Zn	Mg
99.95%	0.03	0.036	0.03	0.001	0.01	0.01	0.02	bal

* The percentage impurities indicated in the table are the maximum possible values. 99.95% is the minimum gauranteed purity.

(c) Copper-aluminum alloy

Aluminum*	7.9%
Copper*	bal.

* Prepared from stock of 99.99+% purity.

(d) 70-30 brass

Lead	0.07
Iron	0.05
Other elements	0.15
Copper	68.5
Zinc	bal.

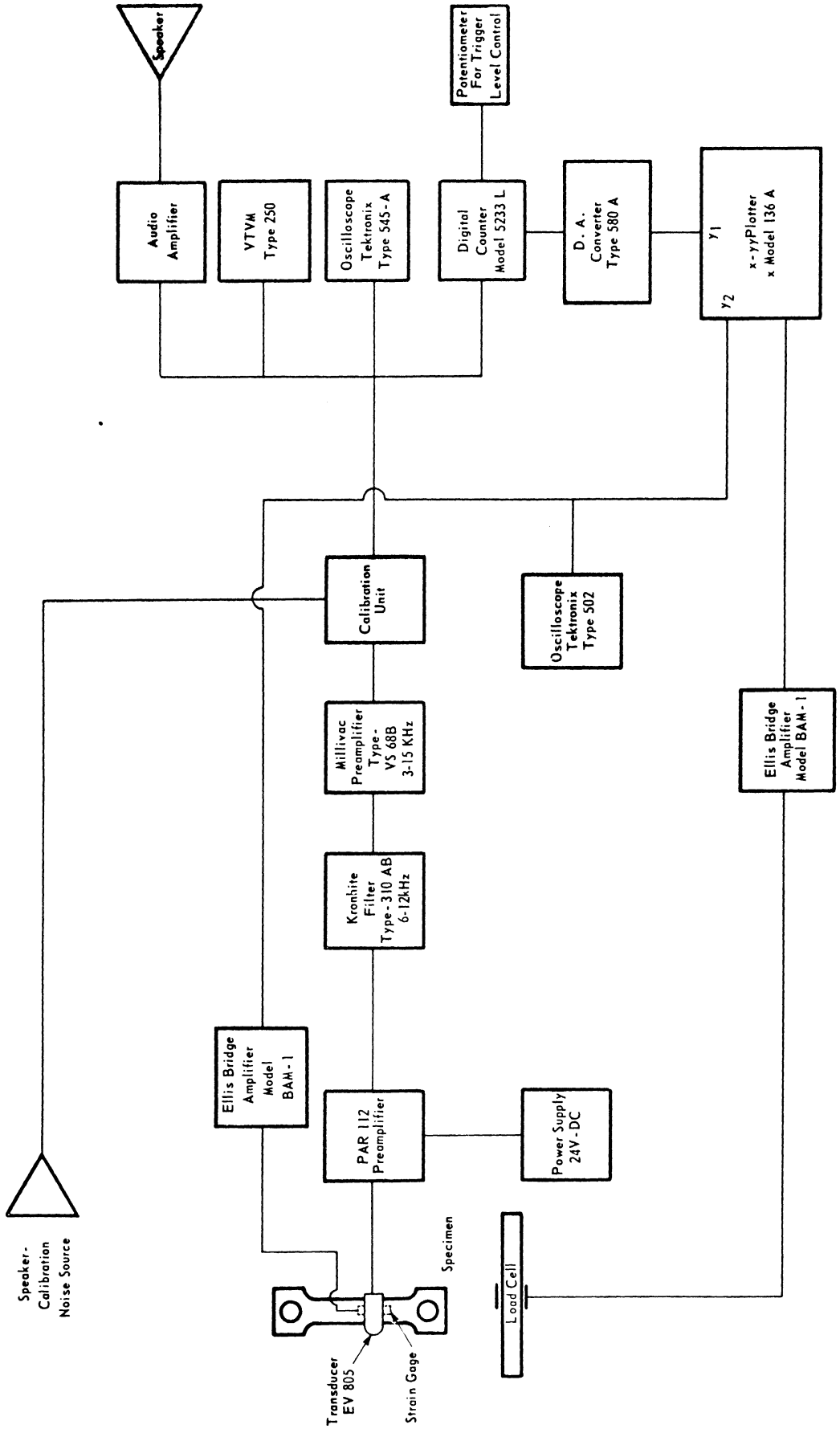

Figure 2 Schematic of the Acoustic Emission Instrumentation System.

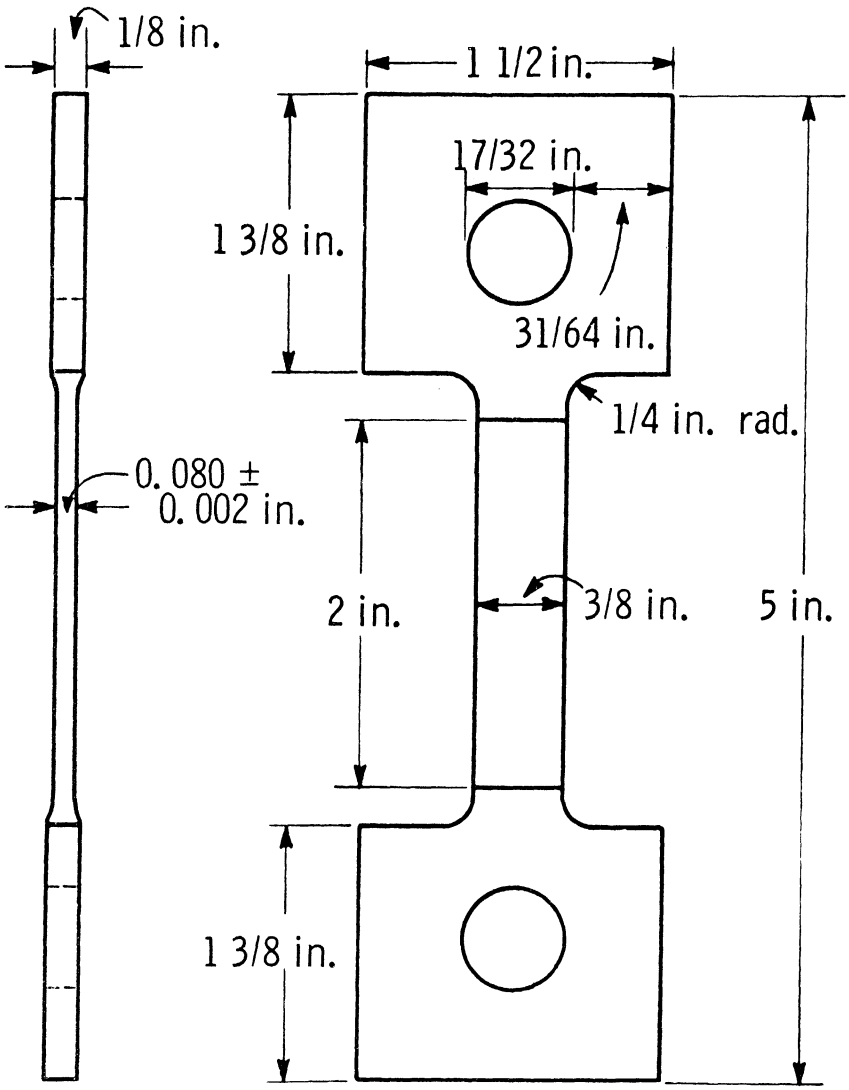

Figure 3 Acoustic Emission Test Specimen.

Fig. 4 shows the acoustic emission data from a sample having an average grain size of 1500 microns. The X-Y recorder pen is automatically reset to zero after every 10,000 counts. This accounts for the appearance of the load emission plot for a total count of 20,800 during the first loading. The arrow (↑) on the abscissa indicates the maximum stress level reached in the previous load-unload cycle. The other arrow (↑) indicates the maximum stress level reached. There is a large amount of load emission of the high-rate type. The unload emission counts are very low and are of the burst type. Fig. 5 shows stress-strain data for this material along with load and unload emission data.

Only very few load emission counts were obtained on the second loading when the previous stress level is not exceeded: 84 counts as compared to 20,800 counts in the first load cycle. The load emission activity of high-rate type commences on loading when the previous stress level is exceeded in the second loading. A preload of 37.5 lb. was maintained on the specimen to minimize emission from the interface between the specimen and the grips.

Specimens with different grain sizes were obtained by cold-rolling as-received one inch diameter bar stock by different amounts and recrystallizing the material. 80% cold work followed by heating at 482°F for 2 1/2 hours resulted in a sub-grain size of about 15 microns whereas 50% cold work followed by heating at 662°F for 2 1/2 hours resulted in an average grain size of about 125 microns.

Fig. 6 shows the load and unload emission data from 99.99% aluminum with different grain sizes. The specimen shown at Fig. 6 (a) has an average grain size of 125 microns and that shown at Fig. 6 (b) has a size of about 15 microns. Specimen (b) showed no unload emission on reloading

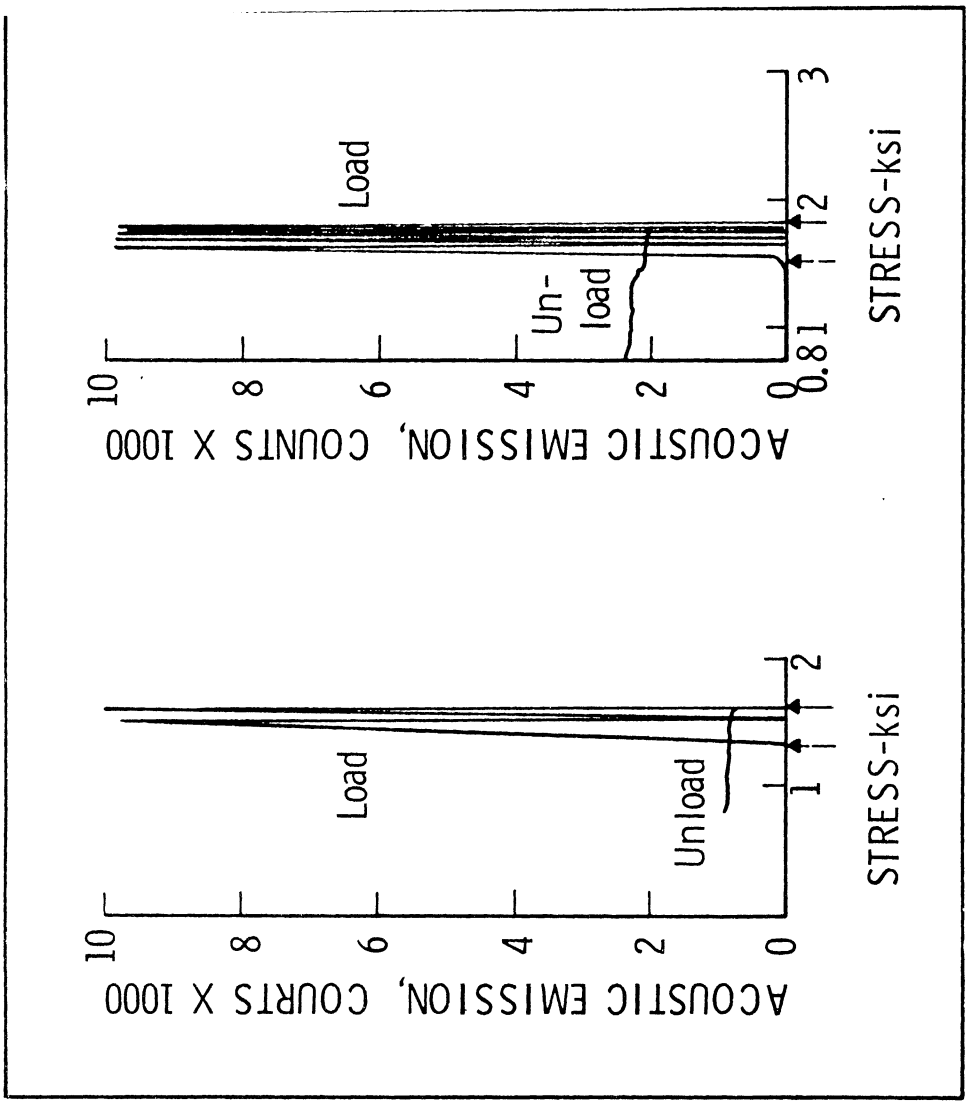

Figure 4 Acoustic Emission from a 99.99% Aluminum Specimen At Two Different Stresses. The Specimen was Annealed at 970°F for 3 Hours. Average Grain Size - 1500 Microns. Hardness 31 R_H.

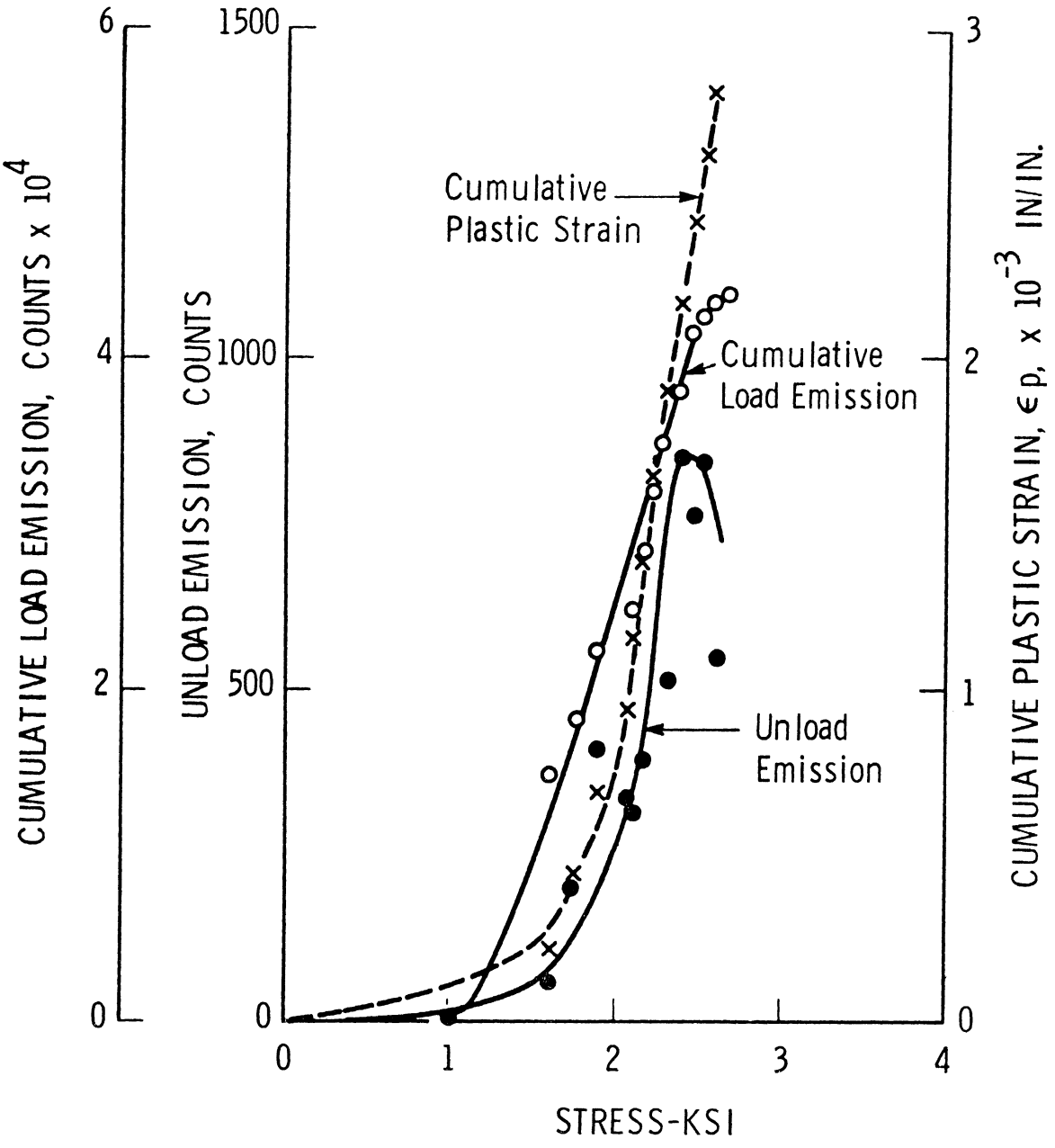

Figure 5 Stress vs Cumulative Load Emission, Unload Emission, and Cumulative Plastic Strain in a 99.99% Aluminum Specimen, Annealed at 970°F for 3 hours, Average Grain Size 1500 Microns; Hardness 31 R_H.

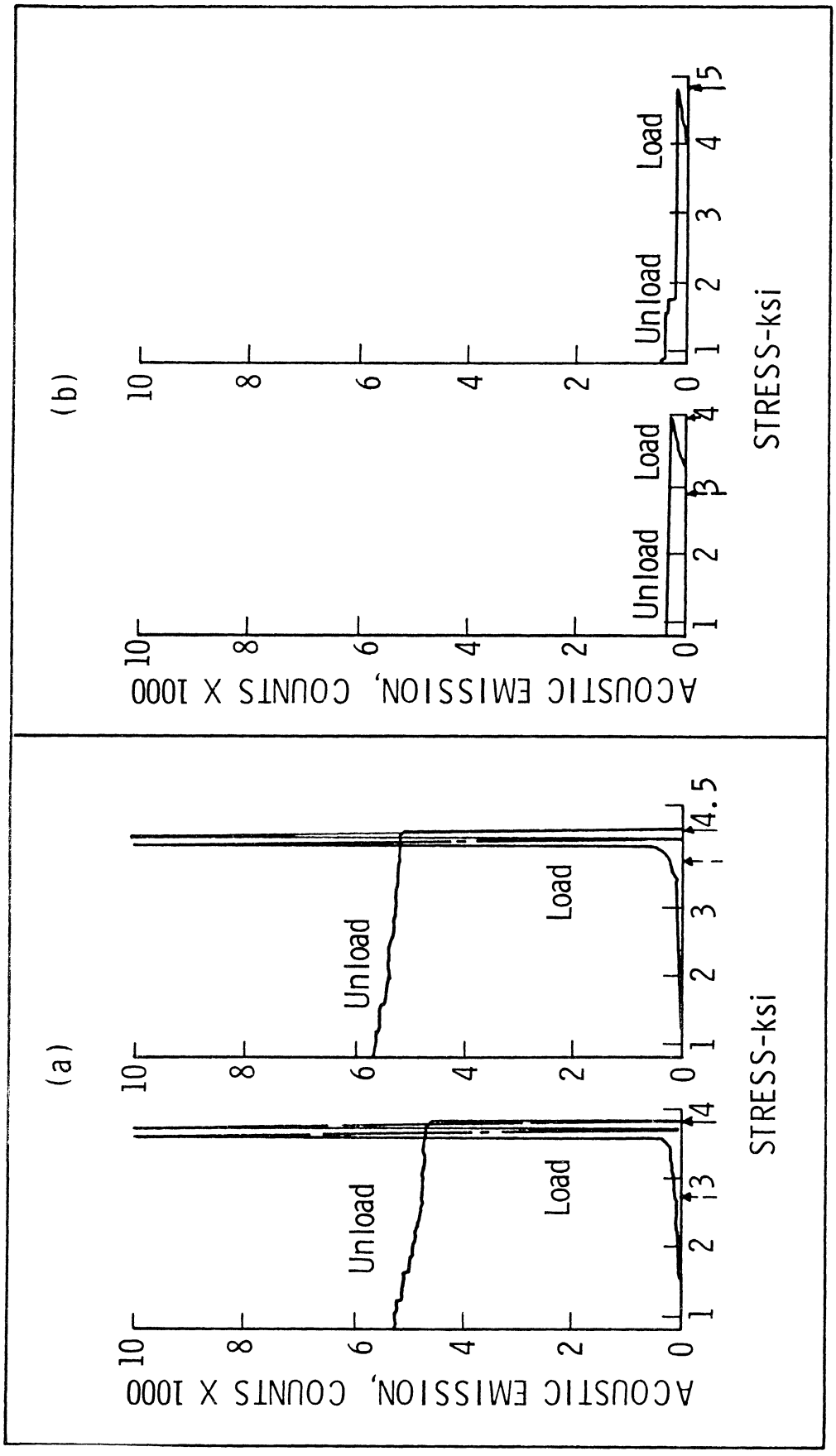

Figure 6 Effect of the Grain Size on the Unload Emission of 99.99% Aluminum Specimens. (a) Acoustic Emission from a Specimen of Average Grain Size of 125 Microns. (b) Acoustic Emission from a Specimen of Average Grain Size of 15 Microns, at Two Different Stresses.

up to the previous stress level whereas the large-grain specimen (a) showed the high-rate type of emission on loading and the burst type of emission on unloading. Fig. 7 shows a plot of stress vs unload emission for samples of both grain sizes.

4.2 Emission Behavior of 6061 and 2024 Aluminum Alloys

Test specimens were machined from sheet stock and annealed at 970°F for three hours and furnace cooled.

Figs. 8 and 9 show stress vs strain, load emission and unload emission for 6061 and 2024 alloys respectively.

Tests were conducted on 6061 alloy with different aging treatments in order to observe the effect of hardness on the unload emission. Five identical specimens were solution treated by heating at 970°F for 3 hours. Aging was done at 400°F for different lengths of time. The resulting hardness values are shcwn in Table II. All the specimens were subjected to a maximum stress of 6600 psi in one load-unload cycle. Fig. 10 shows the effect of hardness on unload emission for the differently heat-treated specimens.

An effort was made to determine if a correlation exists between the unload emission of 2024 aluminum alloy with different aging treatments and the corresponding Bauschinger effect. Four specimens of 2024 aluminum alloy were solution treated by heating at 970°F for three hours. The aging treatments and the hardnesses attained are shown in Table III. All the specimens were subjected to a maximum stress of 8250 psi in one load-unload cycle. Table III also shows the emission response. As aging progresses, acoustic emission decreases, goes through a minimum value, and then increases.

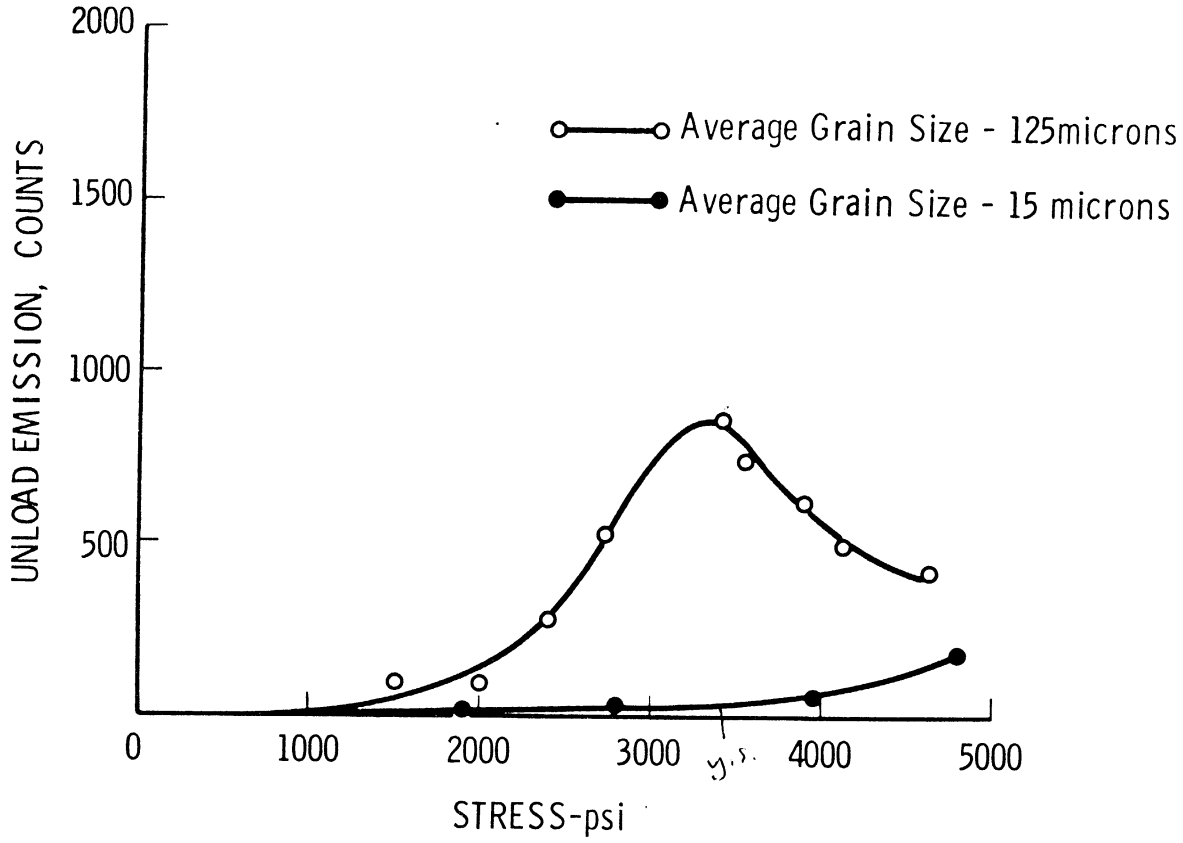

Figure 7 Effect of the Grain Size on the Unload Emission of 99.99% Aluminum.

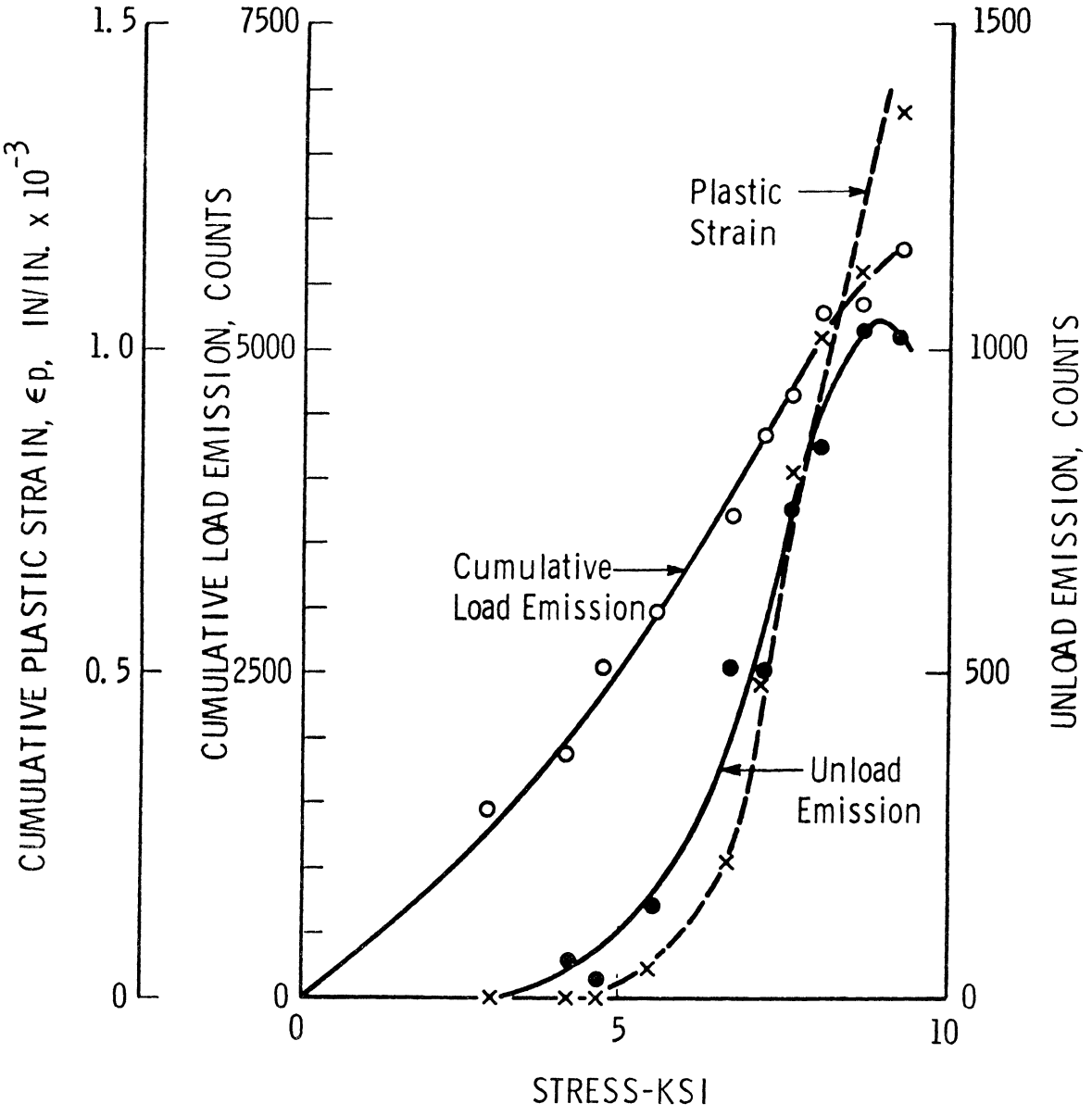

Figure 8 Stress vs Cumulative Load Emission, Unload Emission and Cumulative Plastic Strain in a 6061 Aluminum Alloy Specimen, Annealed at 970°F for 3 Hours. Average Grain Size 55 Microns; Hardness 15 R_E.

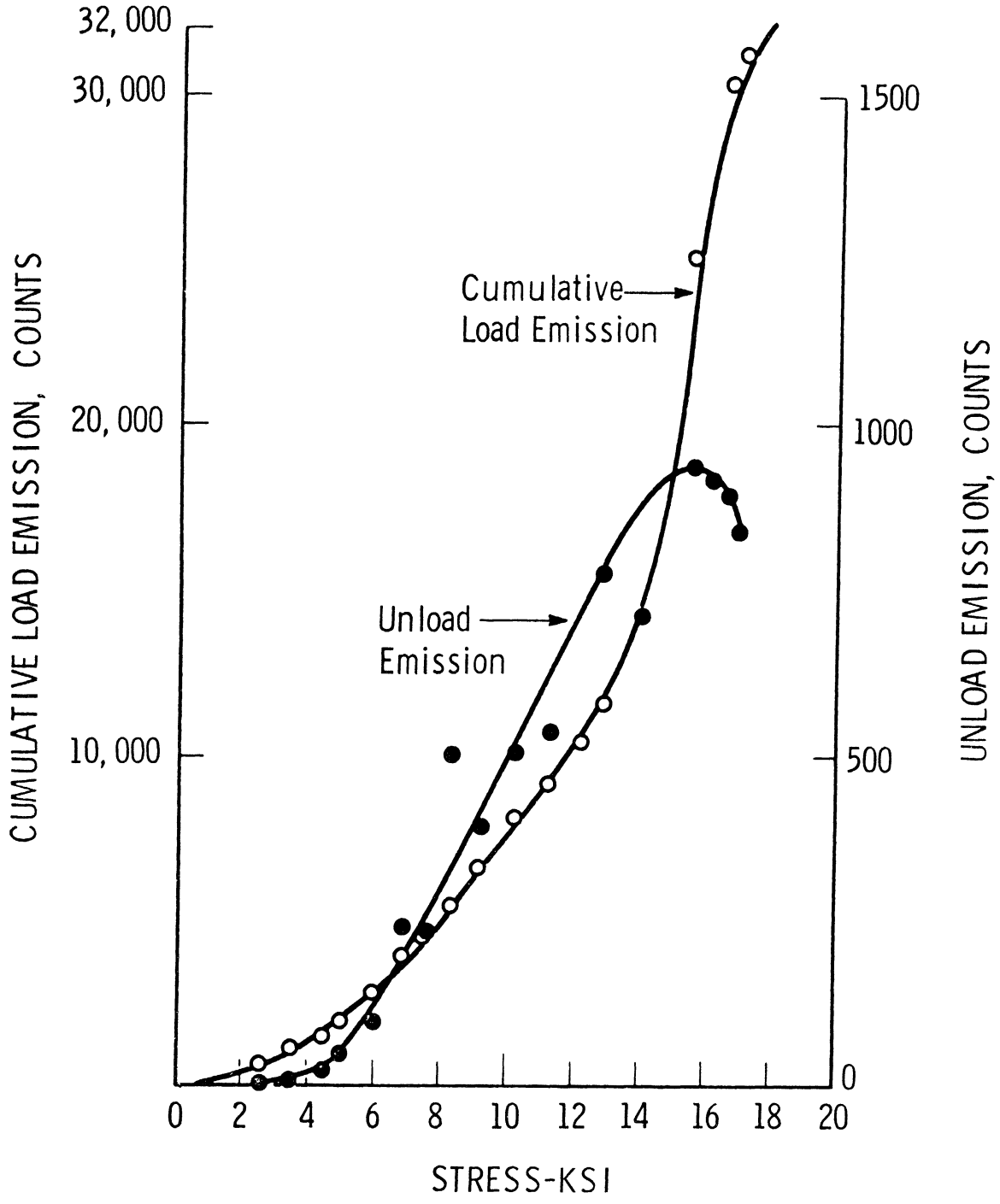

Figure 9 Stress vs Cumulative Load Emission, and Unload Emission in a 2024 Aluminum Alloy Specimen, Annealed at 970°F for 3 Hours. Average Grain Size 110 Microns; Hardness 65 R_E.

TABLE II

AGING TIME AND RESULTANT HARDNESS OF 6061 ALUMINUM ALLOY

Specimen No.	Aging Time at 400°F in Hours	Hardness, R_E
81	0	36
82	1.5	94
84	24	87
85	49	84
86	144	82
87	373	72

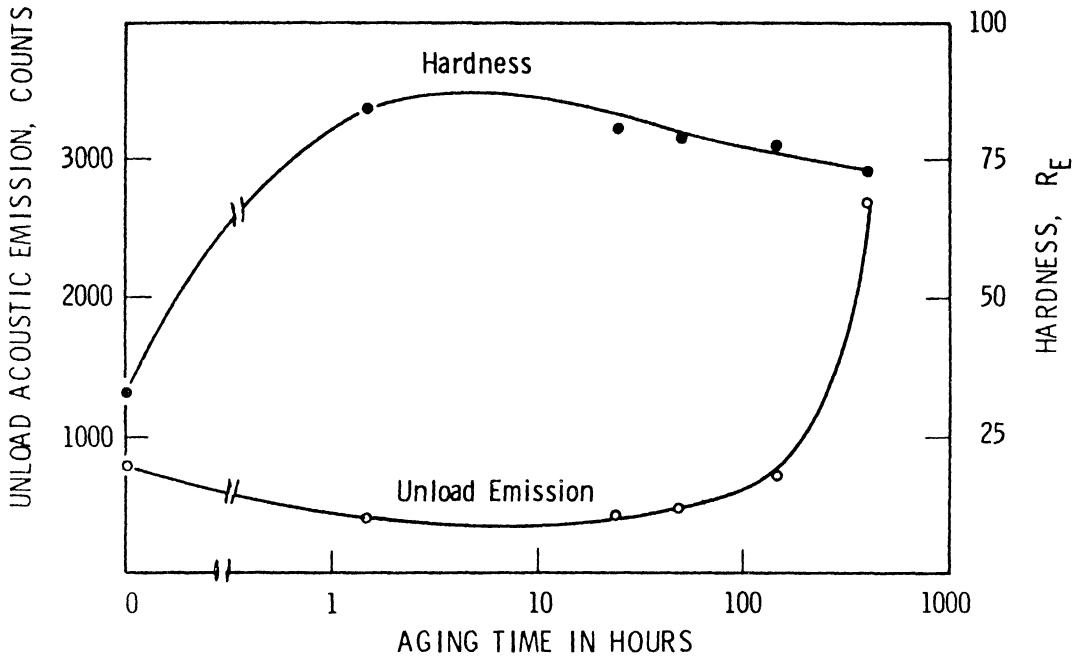

Figure 10 Aging Time vs Unload Emission and Hardness for 6061 Aluminum Alloy Specimens. The Specimens were Aged at 400°F for Different Periods of Time. All the Specimens were Subjected to a Maximum Stress of 6600 psi.

TABLE III

AGE-HARDENING TREATMENT, HARDNESS, THE RESULTANT MICROSTRUCTURE AND THE UNLOAD EMISSION IN 2024 ALUMINUM ALLOY

Specimen No.	Aging Treatment	Hardness R_E	Microstructure	Unload Emission, Counts
71	264°F for 16 Hrs.	100	G-P Zones	697
72	320°F for 5 Hrs.	103	θ'' Precipitate	562
73	428°F for 5 Hrs.	101	θ' Precipitate	621
74	572°F for 5 Hrs.	91	θ Precipitate	715

4.3 Emission Response of Copper-Aluminum Alloy

A copper-7.9% aluminum alloy was chosen as a test material because it exhibits a large Bauschinger effect.[3] The alloy, prepared from base elements of 99.99% purity was supplied by the Scientific Laboratory of the Ford Motor Company in the form of a 3/4 in. rod. Sheet specimens, 1/8 in. thick, were made from this stock by rolling, and test specimens were machined from the sheet. They were then annealed by heating at 1022°F for 24 hours. Fig. 11 shows the plot of stress vs strain, load, and unload emission.

This material exhibits a large load emission. The emission is of the burst type. The unload emission is quite large, about 3 to 5 times that observed in 2024 aluminum alloy with comparable hardness, subjected to the same maximum stress. The unload emission is also of the burst type. One of the interesting observations in this alloy is the absence of the Kaiser effect, i.e., there is a considerable amount of load emission even before the previous maximum stress level is reached in repeated loading. This emission was found to increase with increasing stress as seen in Fig. 12.

4.4 Emission Response of High Purity Magnesium

If a copper-7.9% aluminum alloy exhibiting planar glide gives considerable acoustic emission on unloading, it might be expected that an hcp material, with slip confined to basal planes, would also show large unload emission. 99.95% magnesium with its tensile axis parallel to the rolling direction has the least chance of the occurrence of a twinning mode of deformation,[4] and so specimens annealed of this material were tested. Fig. 13 shows the load and unload emission behavior. Both the load and the unload emissions are of the burst type. The bursts are of high

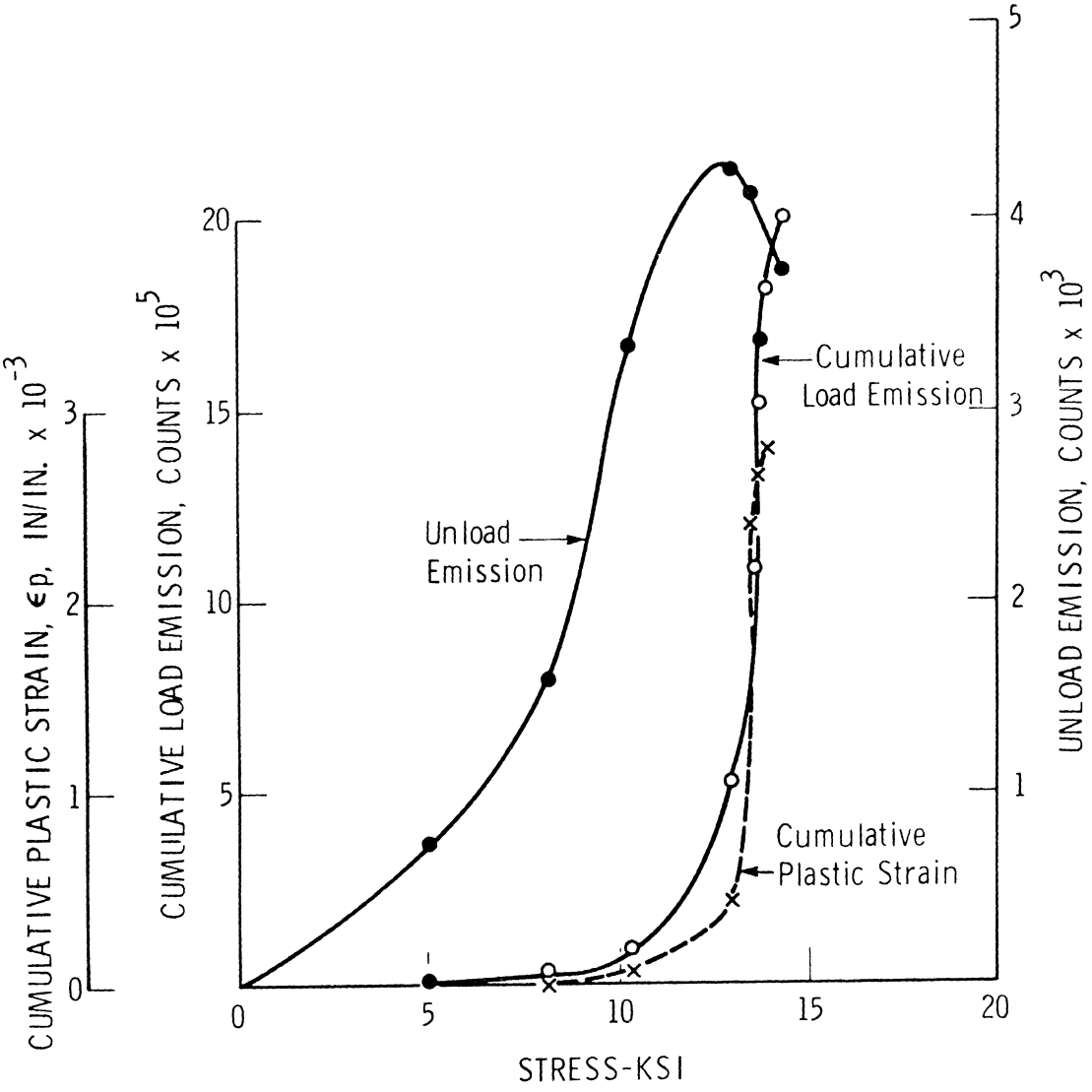

Figure 11 Stress vs Cumulative Load Emission, Unload Emission, and Cumulative Plastic Strain in a Copper-7.9% Aluminum Alloy, Annealed at 1022°F for 24 Hours. Average Grain Size 40 Microns; Hardness 67 R_E.

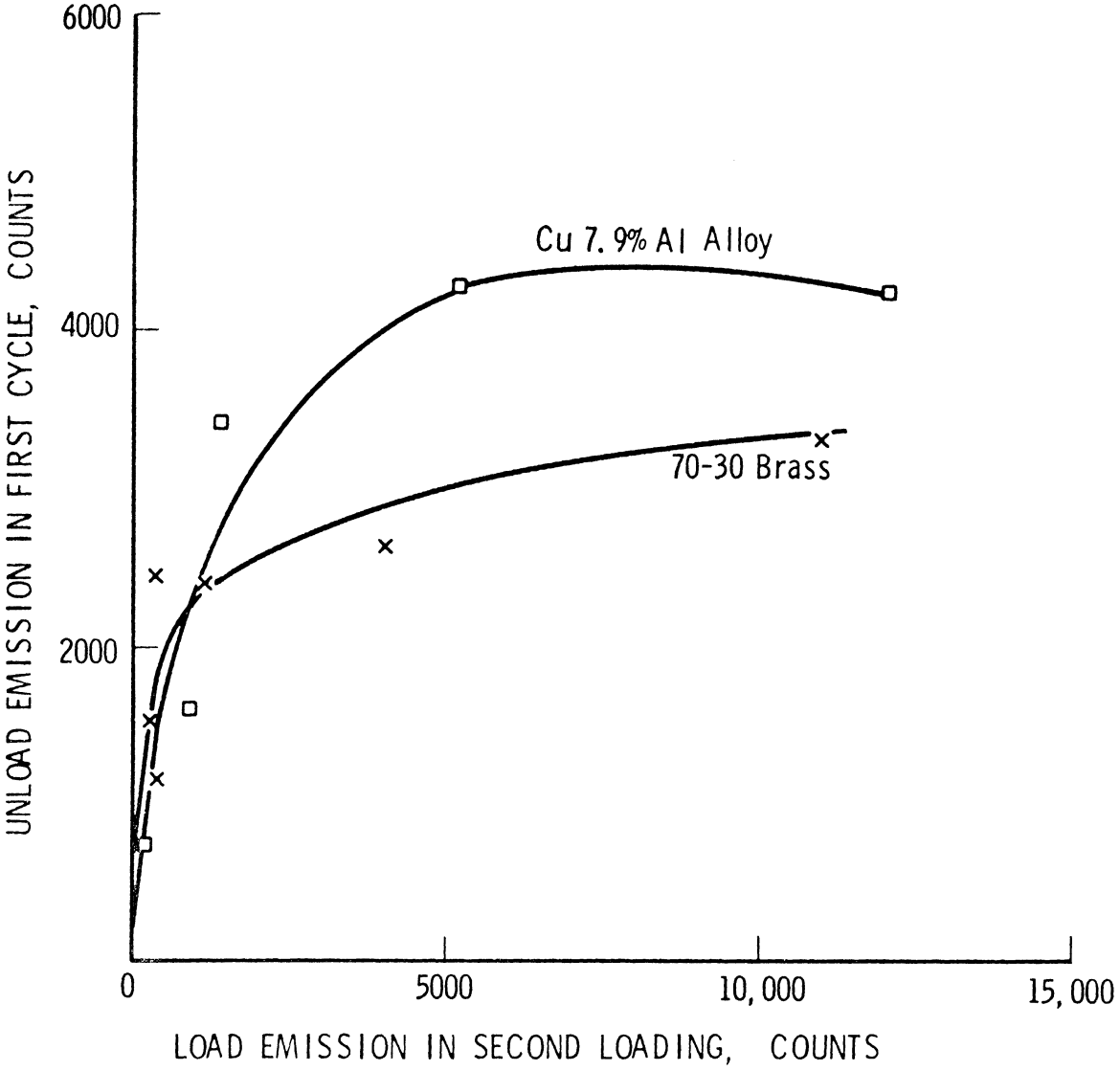

Figure 12 Load Emission in Second Loading vs Unload Emission in Certain Annealed Materials.*

*99.99% Aluminum, 6061 and 2024 Aluminum Alloys do not Show Reverse Load Emission

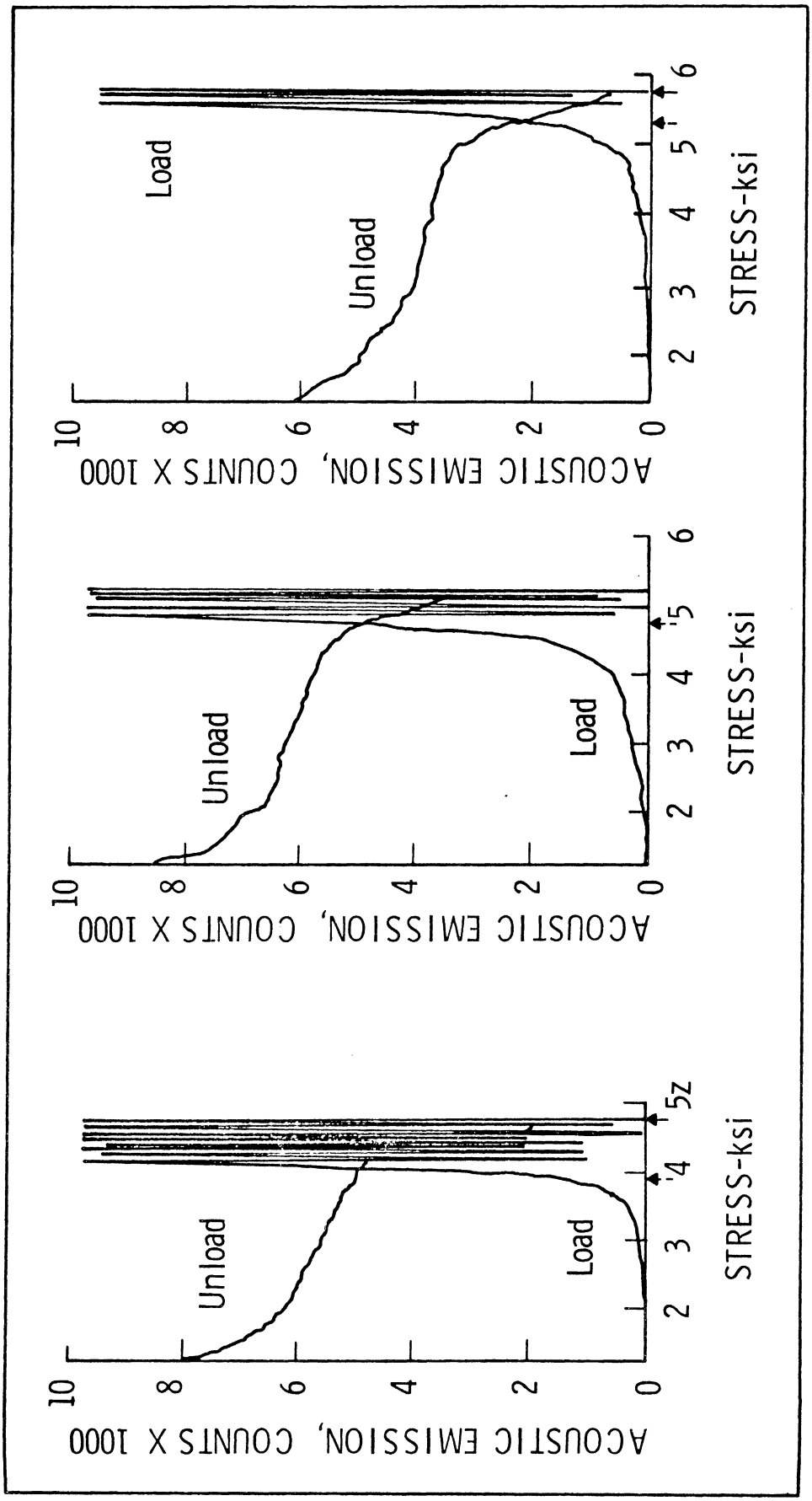

Figure 13 Acoustic Emission from a 99.95% Magnesium Specimen at Three Different Stresses.

The Specimen was Annealed at 700°F for 3 Hours. Average Grain Size 100 Microns; Hardness 31 R_E.

intensity and produced peak-to-peak voltages reaching as high as 65 microvolts. (Ambient noise level was 3.8 microvolts). The complete absence of the Kaiser effect can be very clearly seen.

Since considerable noise can result from twinning it was decided to estimate the contribution of twinning to the strain. Hence, after being subjected to the maximum load, the specimens were chemically polished and etched. The result was that only a few grains showed twin bands. The strain due to twinning was therefore concluded to be less than 10% of that due to slip.

4.5 Emission Response of 70-30 Brass

Samples of commercially available 70-30 brass were annealed at 1022°F for 24 hours. Fig. 14 shows plots of stress vs strain and stress vs load and unload emission. During both loading and unloading the emission is of the burst type. The emission that results from repeated loading can be seen from the results.

4.6 Bauschinger Tests

Since it is felt that unload emission and the Bauschinger effect are very much related, tests were conducted on all the materials used in the acoustic emission study to determine the Bauschinger strain. Fig.15 shows how the Bauschinger strain is determined from the tension, compression stress-strain data. Bauschinger test specimens were made from different materials with same chemical composition as acoustic test samples. All the specimens were tested in the annealed condition, the heat treatments being identical to the ones given to the acoustic test samples. The specimens were subjected to a tensile load so that the total strain in each specimen was 0.005 in./in. unloaded, and then subjected to a compressive

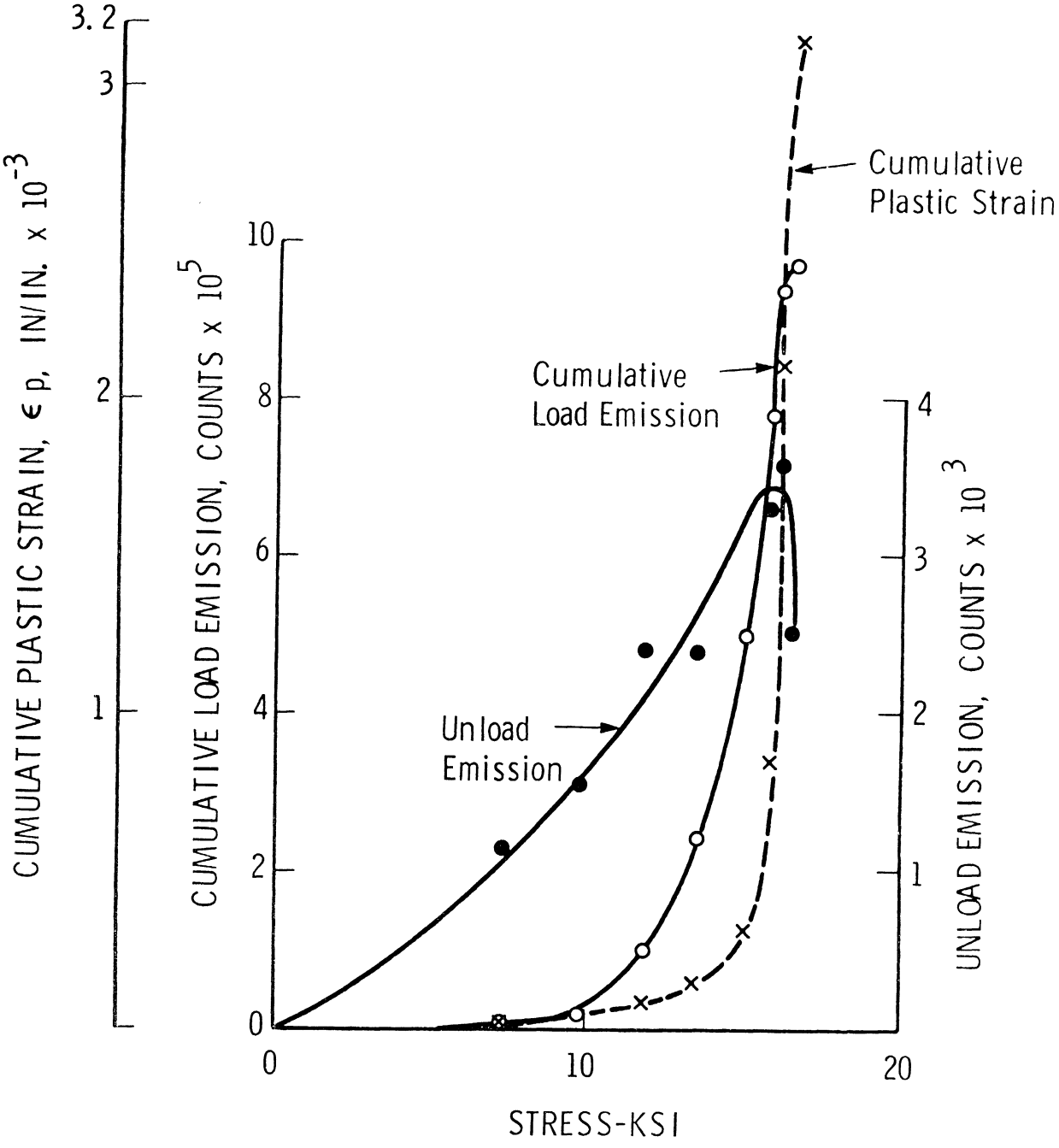

Figure 14 Stress vs Cumulative Load Emission, Unload Emission and Cumulative Plastic Strain in a 70-30 Brass Specimen, Annealed at 1022°F for 24 Hours. Average Grain Size 50 Microns; Hardness 72 R_E.

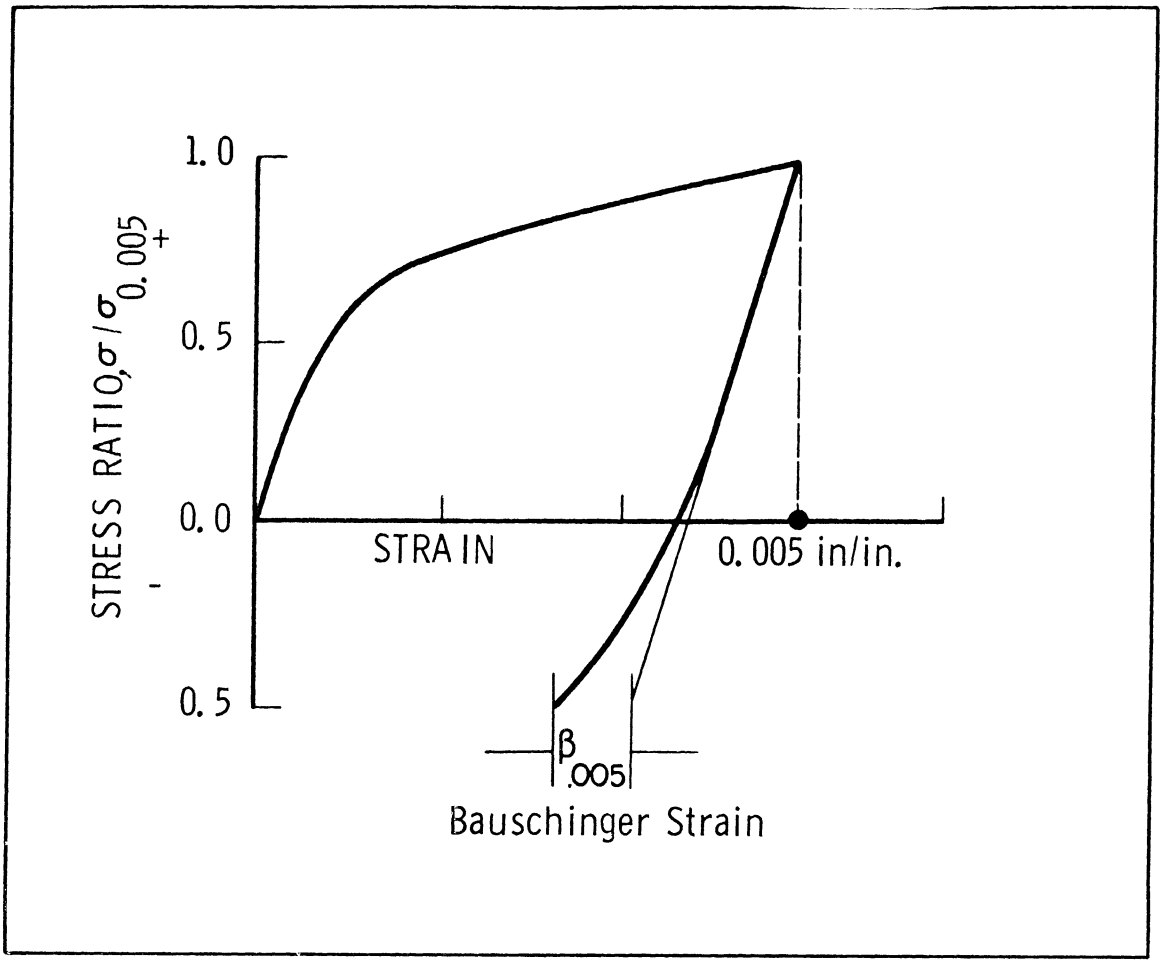

Figure 15 Method for Calculating the Bauschinger Strain from the Tension-Compression Load Test Data.

loading. The maximum compressive stress was kept at 50% of the maximum tensile stress. Instead of plotting the usual stress-strain curve, the ratio $\sigma/\sigma_{0.005}$ is plotted as a function of strain, where σ is the stress at any time during loading or unloading and $\sigma_{0.005}$ is the stress necessary during loading in order to give a strain of 0.005 in./in. Fig. 16 shows the results. Fig. 17 shows the Bauschinger effect in 2024 aluminum alloy heat-treated to give different microstructures. The heat treatments are similar to the one given to the acoustic samples.

5.0 Discussion

5.1 Conditions to Produce Reverse Plastic Strain

One of the principal mechanisms of plastic deformation in crystalline solids is slip. Slip is the result of dislocation motion. Upon the application of a stress, either the already existing dislocations can move, or new dislocations can be generated by a mechanism such as a Frank-Read source. As long as mobile dislocations are available, deformation by slip takes place even at very low stresses. Young[5] observed dislocation motion at a stress as low as 5.6 psi in single crystals of copper. Kopenaal[6] measured a stress of about 100 psi to give a strain of 1×10^{-6} in./in. in a copper-5% aluminum alloy.

The following discussion on the conditions necessary to initiate reverse plastic deformation on unloading is due to Cottrell[7], Nabarro[8], and Kulhmann[9].

To initiate motion of an already existing dislocation in a polycrystal, a stress σ_i acting on the dislocation has to be overcome. σ_i is the maximum value of the fluctuating internal stress field, which is the result of the resistance to the motion of the dislocations caused by various irregularities such as foreign atoms, precipitated particles and other dislocations. The

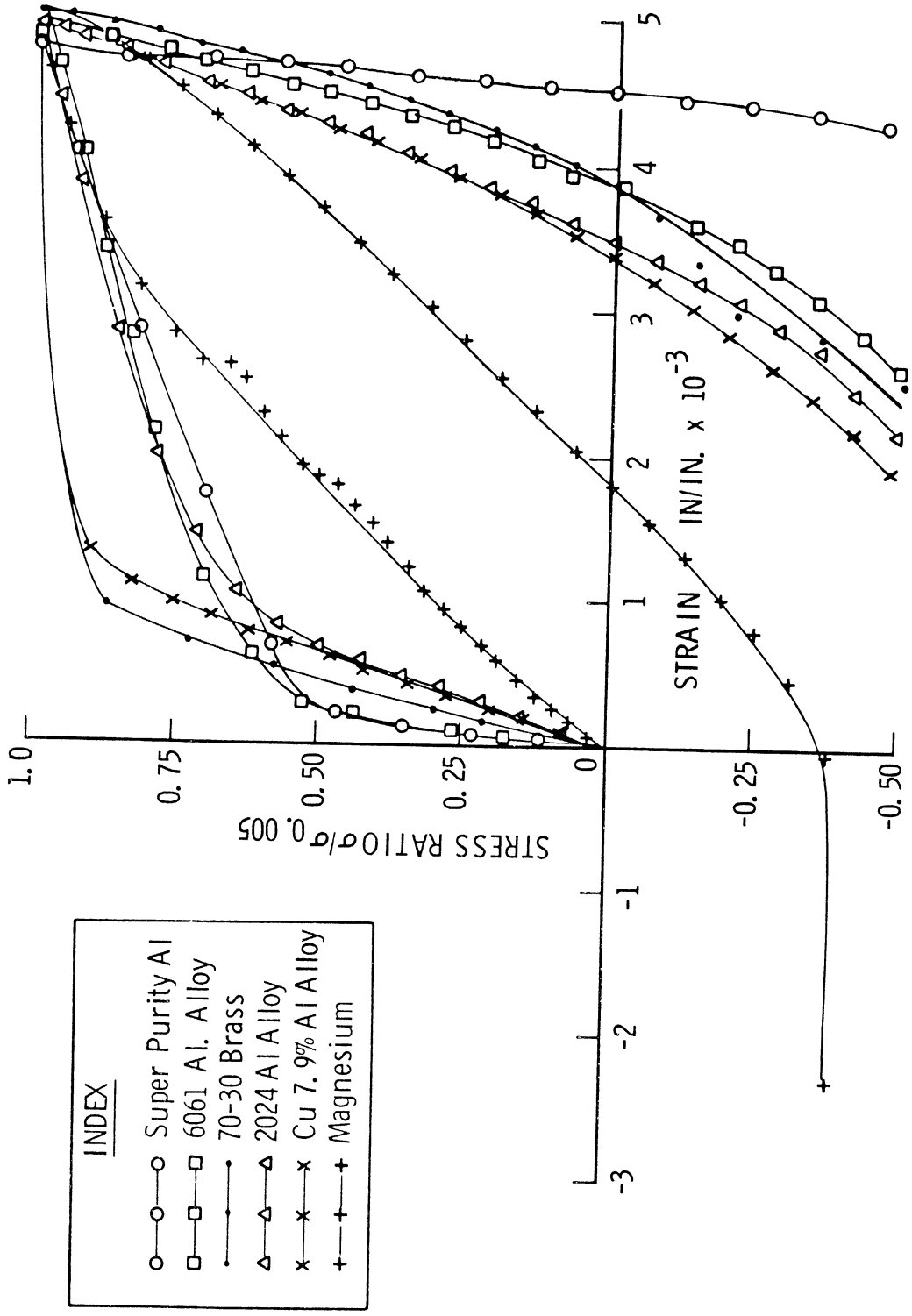

Figure 16 Bauschinger Effect in Several Annealed Materials.

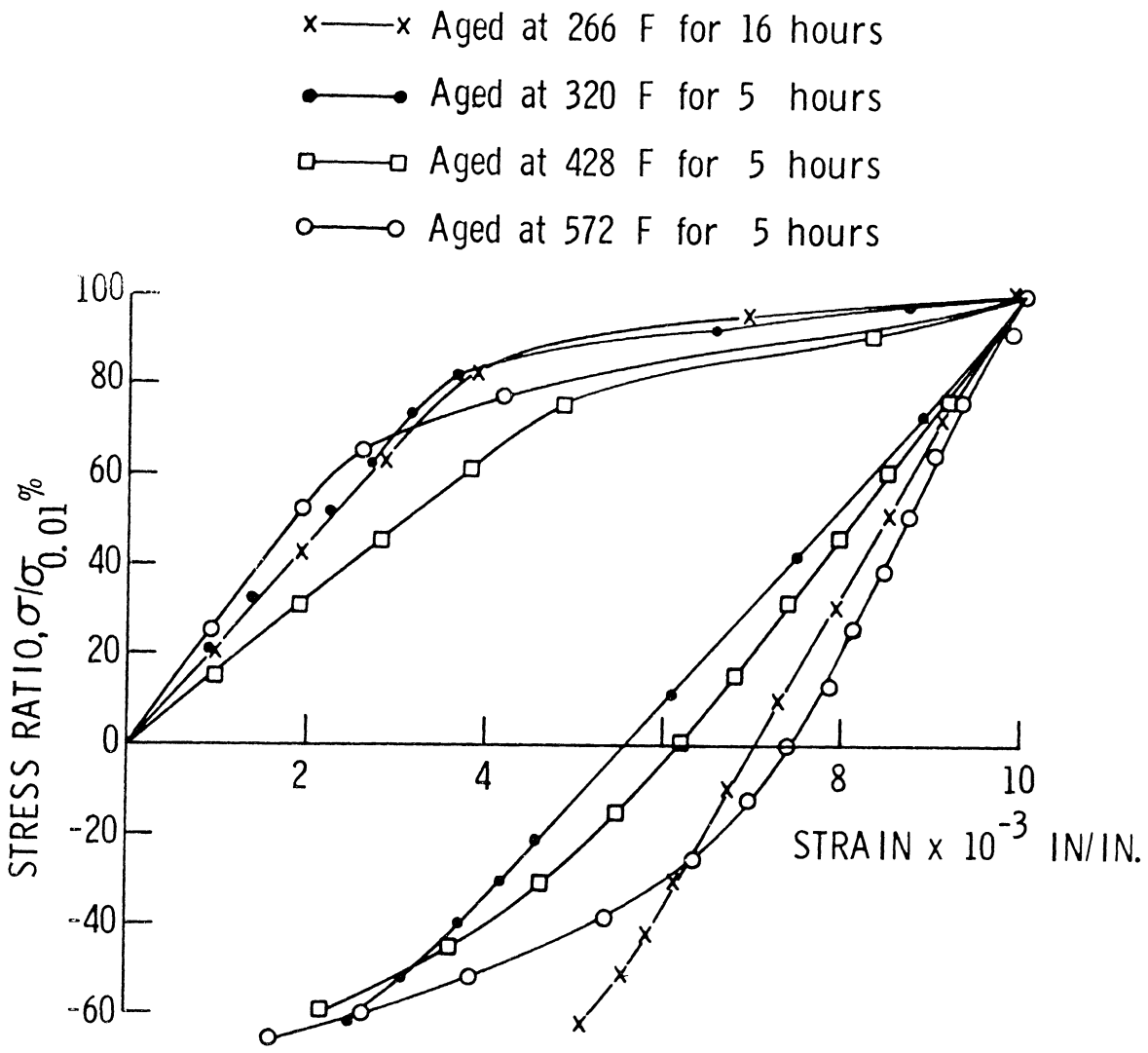

Figure 17 Bauschinger Effect in 2024 Aluminum Alloy Specimens. The Specimens were Solution Treated at 970°F for 3 Hours and Aged at Different Temperatures for Varying Periods of Time to give Different Microstructures.

dislocations can be assumed to be moving through a potential field of energy hills and valleys of constant maximum slope σ_i. When the applied stress σ_1 exceeds the internal stress field σ_i, slip takes place. Dislocations tend to pile up against either obstructions that already exist such as a grain boundary, or those that are created due to dislocations in different planes intersecting, such as Lomer-Cottrell locks. Let σ_d be the back stress due to dislocation pileups at the obstacles. The dislocations have moved forward until

$$\sigma_1 = \sigma_i + \sigma_d \tag{1}$$

Consider what happens when the applied stress σ_1 is reduced to $\sigma_1-\Delta\sigma$. If $\Delta\sigma$ is less than $2\sigma_i$ the dislocations move no farther than across one valley. The internal stress decreases from σ_i to $\sigma_i-\Delta\sigma$ to restore equilibrium. The minimum value to which the internal stress can reduce to is $-\sigma_i$

$$\sigma_1-\Delta\sigma = \sigma_d-\sigma_i \tag{2}$$

From (1) and (2) it is clear that as long as the dislocation motion is limited to the distance across one valley, the resulting plastic strain is small.

When the reduction in the applied stress $\Delta\sigma$ is greater than twice the value of the internal stress field, i.e. $\Delta\sigma>2\sigma_i$ equilibrium can only be restored by a reduction in the value of the back stress σ_d. This means the dislocation had to move farther than across one valley. The resulting plastic flow is easily perceptible. Thus the only condition to be satisfied to cause reverse flow is $\Delta\sigma>2\sigma_i$.

It can easily be seen that if $\sigma_i>>2\sigma_i$ and the applied stress is then reduced to zero, reverse plastic flow can take place during unloading as shown in Fig. 18.

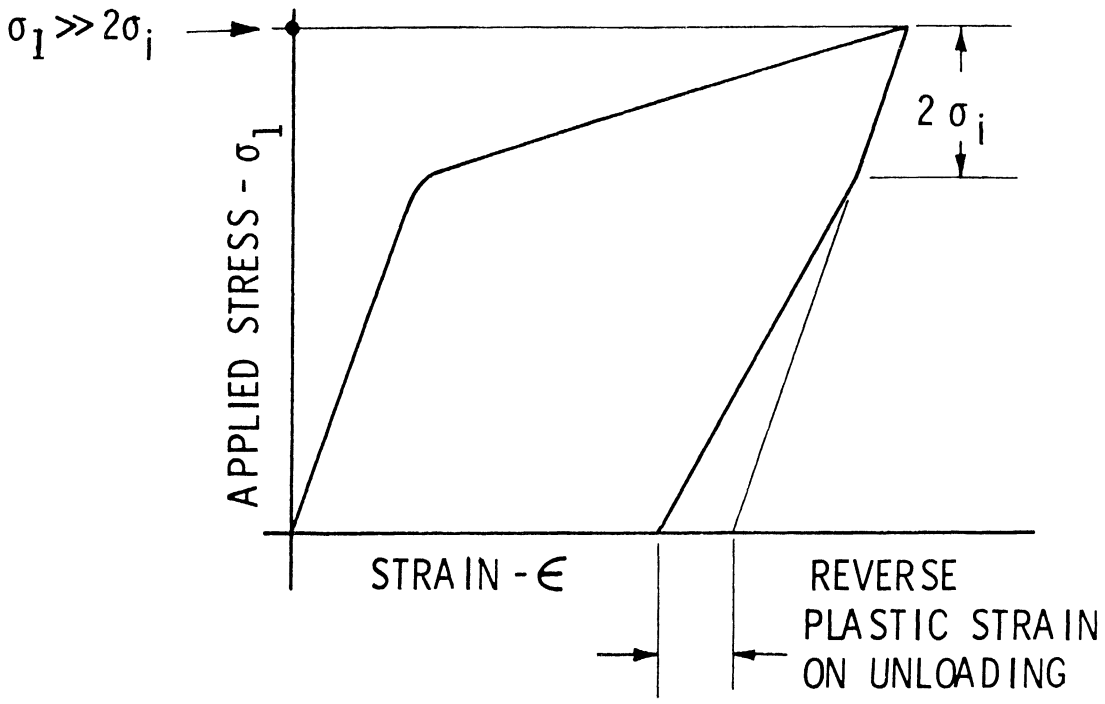

Figure 18 Reverse Plastic Flow on Unloading.

Next consider the forces resisting the motion of dislocation in a little more detail. Contributions to this arise from the following:

1. The resistance offered to the dislocation motion between two successive equilibrium positions, i.e., the force required to overcome the potential separating the two equilibrium positions, a lattice spacing apart. This is the Peierls-Nabarro force.

2. The resistance due to point defects in the lattice, precipitate particles and other dislocations. The spacing of these defect sites is much larger than one atomic spacing.

3. The resistance offered to dislocation motion by grain boundaries and sub-grain boundaries.

A resistance can act as a friction stress or a back stress during the process of unloading, depending upon the extent of dislocation motion. If the motion is limited to two successive equilibrium positions of dislocations, a lattice spacing apart the interaction stress will be a back stress and the only friction stress will be the Peierls-Nabarro stress. If we consider the long range motion of dislocations shearing through several barriers such as precipitate particles, the internal stress due to particles will act more like a friction stress. It can be assumed that at small ranges of stress, slip is limited to within the grains and the resistance that a grain boundary offers becomes more of a back stress. Deak[10] classifies this as a "long-range" back stress whereas back stress due to closely spaced point defects are termed "short-range" internal stresses.

During the process of deformation, it is likely that some dislocations are stopped by closely spaced point defects. Many more may get piled up against strong barriers such as grain boundaries. While unloading,

the short range back stresses relax first as they have to overcome only the Peierls-Nabarro force. It is useful to calculate the order of strain that results when the short range back stresses relax. This simply means that the dislocation motion is limited to motion over a distance lying in between the defects.

The spacing of solute atoms in a solid solution is given by[11]

$$\Lambda = b/c^3$$

where Λ = spacing of solute atoms

c = concentration of solute

b = Burgers vector

We can calculate the strain when the dislocation moves in between two solute atoms. Since the strain that results due to motion of a dislocation between two solute atoms spaced a few atomic distances apart is smaller than that due to motion of the dislocation between incoherent precipitate particles in an overaged alloy, the following calculations are done for an overaged alloy. The results will indicate that unless several dislocations move at one time or one dislocation moves through several particles, even inter-particle motion cannot be detected.

Let us assume a 2 micron spacing between particles in an overaged alloy. Let the dislocation move through an average distance of 1 micron, under the application of a stress. The resulting shear strain

$$\gamma = N'.b.A_s$$

where N' = number of mobile dislocations, per unit volume,

b = Burgers vector, and

A_s = area swept by a unit length of dislocation

For one single dislocation, with an average displacement of 1 micron, the shear strain is $\gamma = 1\ (2.83 \times 10^{-8})\ (1 \times 10^{-4}) = 2.83 \times 10^{-12}$

In an undeformed specimen of annealed aluminum, the dislocation density is of the order of 10^5 to $10^6/cm^2$. If we assume a dislocation density of $10^6/cm^2$ between two precipitate particles spaced two microns apart, the number of dislocation lines is less than one. It can thus be seen that the number of available mobile dislocations is small and so is the strain.

The minimum strain detection capability of the acoustic emission instrumentation used in this investigation is 0.85×10^{-10} in./in. Hence intra-particle motion of the dislocation is unlikely to be detected unless motion between several particles takes place at one time. Thus the major contribution must be due to the relaxation of long range back stresses when the dislocations pile up against the grain boundaries and move through or around several particles. This is contrary to Deak's[10] hypothesis.

5.2 Role of Cross-slip in Reverse Plastic Deformation

The above argument for reverse plastic deformation implies a basic assumption, i.e., that there are enough mobile dislocations in the slip plane to give the deformation on unloading.

At the start of the third stage or near the end of the second stage of deformation, Seeger[12] observed coarse slip in copper and aluminum replicas. At this stage, the slip lines cluster together to form bands which are comparatively short and connected to other bands by slip. The connecting slip is called cross-slip. This is a characteristic feature in the deformation of aluminum. Obstructions to dislocation motion such as Lomer-Cottrell locks in the primary slip planes cause screw dislocations or screw components of edge dislocation loops to cross-slip to alternate planes which have a common slip direction. The ease of cross-slip depends

on the stacking fault energy of the material. To cross-slip, the two partial dislocations have to first come together to form one dislocation. In the case of a metal with low stacking fault energy, the partials are widely separated and the energy needed to force the partials together is higher. Hence cross-slip does not take place easily. On the contrary, aluminum, with a stacking fault energy of about 200 ergs/cm^2 [13] exhibits cross-slip even under low stresses at room temperature.

Seeger[14] obtains the following expression for the shear stress necessary to combine two partial dislocations at the head of a pile-up of dislocations and thus initiate cross-slip.

$$\tau = \frac{1}{n}\left[\frac{\sqrt{2}\,G}{4\pi} - \frac{2\gamma_s}{b}\right]$$

where τ = shear stress necessary to initiate cross slip,

n = number of dislocations in the pile up

G = shear modulus,

γ_s = stacking fault energy, and

b = Burgers vector.

The number of dislocations in the pile up is given by

$$n = \frac{\pi\tau L}{Gb}$$

where L is the maximum glide distance. L is approximately equal to half the grain diameter 'D' in a high purity material. Precipitate particles, subgrain boundaries, etc. reduce the slip distance.

Equation (1) can therefore be written as

$$\tau = \frac{Gb}{\pi\tau L}\left[\frac{\sqrt{2}G}{4\pi} - \frac{2\gamma_s}{b}\right]$$

$$\tau^2 = \frac{Gb}{\pi L}\left[\frac{\sqrt{2}G}{4\pi} - \frac{2\gamma_s}{b}\right]$$

or $$\tau = \sqrt{\frac{Gb}{\pi L}\left[\frac{\sqrt{2}G}{4\pi} - \frac{2\gamma_s}{b}\right]}$$

Certain results are apparent on interpreting the above equation. They are as follows:

1. Larger grain size decreases the shear stress necessary to initiate cross-slip. For the same plastic strain, larger grains will contain a longer pile up and will undergo cross-slip at a lower stress.

2. Higher stacking fault energy allows cross-slip at lower stresses.

3. Any condition that decreases the glide distance increases the stress necessary to initiate cross-slip.

From transmission electron microscope observations, Feltner and Laird[3] defined slip character as planar or wavy depending on the degree to which the dislocations are confined to individual slip planes. Aluminum, aluminum-magnesium alloys, copper, pure dilute iron-carbon alloys, etc., show wavy slip mode. Copper-aluminum alloys and brass show planar slip mode. Feltner and Laird[3] observed a dislocation structure that is confined to one plane in a copper-7.5% aluminum alloy subjected to cyclic stresses. No dislocation dipoles were observed. Also 70-30 brass, cyclically strained at smalle amplitudes, showed straight dislocations forming many multipoles. For very small plastic strains, few complex dislocation interactions occur. On unloading, the short range internal stresses move the dislocations over their own debris. It is likely that more dipoles are formed by the cross-slip. Therefore, the magnitude of friction stress might increase as the dipole density increases during loading and unloading.

Materials that exhibit planar slip mode show considerable reverse plastic deformation on unloading. Feltner and Laird[2] observed a deformation as high as 15% to 20% of the prestrain in copper-7.5% aluminum alloy, annealed, whereas high purity annealed copper did not show any deformation on unloading. The Bauschinger tests conducted on a copper- 7.5%

The Bauschinger tests conducted on a copper-7.9% aluminum alloy during this investigation confirm this. It can be concluded that the reversal of dislocation motion is much easier in a planar mode material for the following reasons:

1. Slip is confined to primary planes because of reduced cross-slip activity.

2. The dipole obstacle density is very low.

3. The reverse dislocation motion, aided by long range back stresses, takes place easily. The opposite is the case with wavy slip mode materials.

The above discussion on reverse plastic deformation can be summarized as follows:

1. Reverse plastic deformation on unloading is possible if the applied stress exceeds twice the value of the internal stress, i.e., $\sigma_1 >> 2\sigma_i$ and if the decrease in the applied stress $\Delta\sigma$ is greater than twice the value of the internal stress σ_i, i.e., $\Delta\sigma > 2\sigma$.

2. This reverse deformation is considerable in planar slip mode materials because there is less cross-slip and dislocations are thus generally confined to primary slip planes.

3. There is a certain minimum strain pulse that the measuring system is capable of picking up. Hence, the slip in the secondary systems may not be picked up by the detection system.

The above explanation is one among the possible mechanisms that can explain the observed load emission behavior. The increased resistance to dislocation motion due to interaction with forest dislocations might also prevent the dislocations from moving back.

The unload emission behavior of various materials is discussed in the light of the above conclusions.

5.3 99.99% Aluminum, and 6061 and 2024 Aluminum Alloys

From Seeger's[14] equation, the applied stress to initiate cross-slip in a polycrystalline 99.99% aluminum sample, annealed at 970°F for three hours is calculated as being about 800 psi. The average grain size of the sample was about 1500 microns. Among all the materials tested, 99.99% aluminum gave the least unload emission as can be seen in Fig. 19 which compares unload emission behavior of various materials for the same plastic strain. It is more meaningful to compare emission at the same strain as the dislocation interaction can be assumed to be similar for this condition. The low unload emission in high purity aluminum is explained as follows. If other factors do not interfere, slip distances are larger in large grain specimens and there are more strain pulses whose amplitude lies above the detection capability of the measuring system. This is verified by the large amount of acoustic emission obtained during loading in 99.99% aluminum. The ease of cross-slip at lower stresses, however, reduces the availability of dislocations in primary planes which might possibly move back and give rise to reverse deformation. Though friction stresses are low, cross-slip seems to be the predominant factor in controlling the amount of reverse deformation. Fig. 5 shows a drop in unload emission at a stress of about 2200 psi (at a strain approximately equal to 0.2%). This is due to increased cross-slip activity as well as increasing obstructions to dislocations and other forms of frictional stresses.

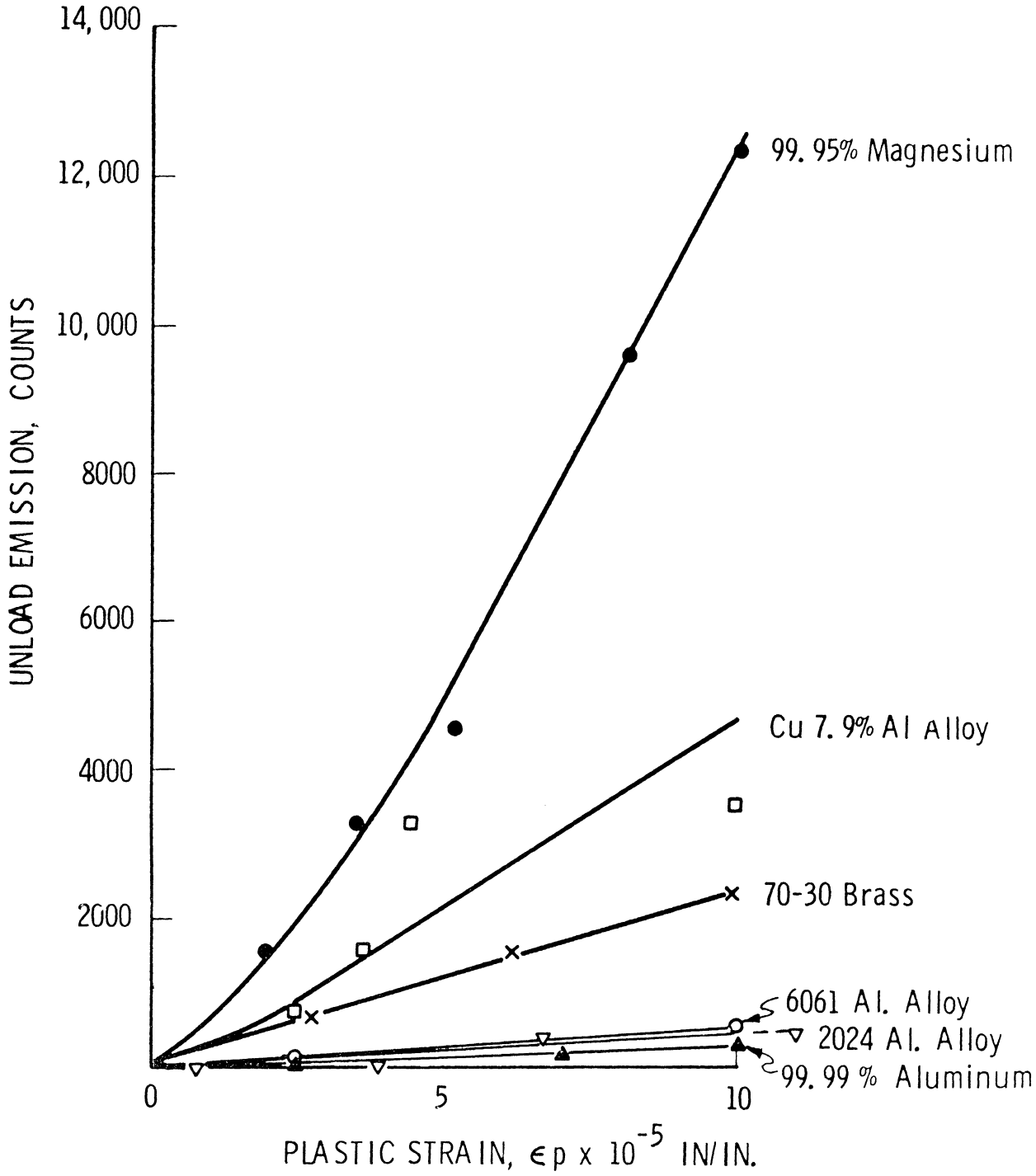

Figure 19 Strain vs Unload Emission for Certain Annealed Materials.

The effect of grain size on the unload emission of 99.99% aluminum is shown in Fig. 7. In large-grain polycrystalline material, the deformation might take place on a single slip system but as the stress is increased, several slip systems become operative. In fine-grained specimens, deformation is essentially by multiple slip. Whereas a large grain specimen shows a decrease in unload emission at a lower stress of about 3100 psi, the unload emission curve for a fine-grain specimen shows no drop in emission activity within the stress levels used in this investigation, as can be seen in Fig. 7, even though a much smaller number of emission counts is involved. Slip takes place in smaller strain increments in fine-grain samples.

For the 125 micron grain size sample, the applied stress to initiate cross-slip is about 2360 psi. It can thus be assumed that extensive cross-slip activity exists at a stress of about 3000 psi and hence the appearance of a drop in the unload emission beyond this stress level. For the 15 micron grain size sample, the applied stress to initiate cross-slip is about 6750 psi. It is seen from Fig. 7 that the unload emission, though small in fine grained samples does not show a tendency to decrease at stresses as high as 5000 psi.

Another factor might also contribute to the reduction in unload emission counts in large grain material. Segal and Patridge[15] have reported changes in the dislocation density at various stages in uniaxial deformation of 99.99% aluminum. The average density of the dislocations in an annealed specimen is $5 \times 10^6/cm^2$. In specimens stressed up to 1350 psi, most of the regions appear similar to the annealed material. At 2700 psi, there are more regions where the dislocation density is as high as $2 \times 10^8/cm^2$, though there are large regions which still contain no dislocations. However, at about 4000 psi there is a tendency for

dislocations to form groups. The dislocations are also shorter and more numerous. This means that as the deformation proceeds, slip distances become smaller and smaller. It becomes increasingly difficult for the dislocations to move back when the applied stress is relaxed due to more dislocation interaction.

Fig. 19 shows a comparison of the unload emission counts of 99.99% aluminum, aluminum-copper 2024 and aluminum-magnesium 6061 alloys. The aluminum alloys show a slightly larger value of unload emission as compared to 99.99% aluminum. The grain size of these alloys is much smaller than that of 99.99% aluminum. Turnbull[13] gives a value of 117 ergs/cm^2 for the stacking fault energy of an aluminum-1% magnesium alloy. Pure aluminum has a stacking fault energy of about 200 ergs/cm^2 [13]. This, together with increased drag resistance, makes cross-slip more difficult in these alloys. Fig. 8 shows a drop in the unload emission at about 8750 psi for annealed 6061 aluminum alloy. A 2024 aluminum alloy will show cross-slip at much higher stress. Seeger's equation gives a value of 14028 psi as the applied stress to initiate cross-slip in a 2024-T6 aluminum alloy specimen. Fig. 9 shows that the unload emission drops at about 15000 psi in an annealed 2024 aluminum alloy.

The unobstructed slip distance will be largest in supersaturated solid solution and diminishes as the precipitation process commences. This will increase in the overaged condition. Thomas and Nutting[16] report mean slip distances of 3000 Angstroms when the microstructure contains G-P zones, 400 Angstroms when the microstructure contains θ'' precipitate, and 700 Angstroms when it contains the coherent θ' precipitate. When the structure consists of an incoherent precipitate θ,

cross-slip is observed and the slip lines are wavy. Thus the following conclusions can be stated.

1. In the case of solution treated alloys, the slip distances are sufficiently large so the strain pulses are easily picked up by the detection system, whereas the strain pulses are too small when the alloys are aged to produce peak hardness.

2. The tendency for cross-slip is much lower in overaged alloys as is evident from the shape of the hardness vs unload emission curves in the case of 6061 and 2024 aluminum alloys.

It is of interest to compare this result with the Bauschinger effect in 2024 aluminum alloys with different microstructures (Fig. 17), and with the results of Abel and Ham[17] on the effect of microstructure on the Bauschinger effect in 2024 aluminum alloy as shown in Table IV. Table IV indicates the possibility of a relationship between the unload emission and Bauschinger effect in this alloy. However it is to be borne in mind that the fact that there is a deformation on unloading does not necessarily mean that this can be detected by the measuring system. The intensity of the strain pulses must be above the minimum strain detection capability of the system.

5.4 Copper-7.9% Aluminum Alloy

Copper-7.9% aluminum is a single phase alloy and the specimen used in this investigation had a grain size of about 50 microns. The stacking fault energy is approximately 4 ergs/cm^2 [18]. Among the fcc metals and alloys tested, this alloy showed the largest unload emission for the same amount of strain, as can be seen in Fig. 19. The stress to initiate cross-slip is quite high. Electron microscope studies indicates slip to be planar and confined mostly to primary planes. It would therefore be expected that

TABLE IV

BAUSCHINGER EFFECT AND UNLOAD EMISSION IN

2024 ALUMINUM ALLOY HEAT TREATED TO

GIVE DIFFERENT MICROSTRUCTURES

Heat Treatment	Microstructure	Unload Emission	Bauschinger Strain*, Microinches/in.	Percentage Bauschinger Stress#
Aged at 264°F for 16 Hrs.	G.P.zones	697	90	44
Aged at 320°F for 5 Hrs.	θ" Precipitate	562	90	14
Aged at 428°F for 5 Hrs.	θ' Precipitate	621	1120	16
Aged at 572°F for 5 Hrs.	θ Precipitate	715	2080	61

* The Bauschinger strain is calculated at a compressive stress which is 50% of the tensile stress needed to obtain a strain of 0.001inches/in.

Percentage Bauschinger stress is defined as $\frac{\sigma-\sigma_c}{\sigma}$. σ is the highest stress in tensile loading and σ_c = stress to initiate yield in reversed loading. The values of σ and σ_c are taken from Abel and Ham

under the absence of cross-slip, and with less friction stress due to the absence of second phase particles, unload emission should be quite high. This is verified in Fig. 19. The copper-7.9% aluminum alloy showed 3 to 5 times the unload emission that was obtained on a 2024 aluminum alloy of the same hardness, namely about 70 R_E.

5.5 The Kaiser Effect In Copper-7.9% Aluminum Alloy

One of the interesting observations in the copper-7.9% aluminum alloy is the absence of a complete Kaiser effect. Agarwal, Frederick and Felbeck[19] proposed an unstable Frank-Read source as the cause of load emission in aluminum and aluminum alloys. In the case of repeated loading, sources of suitable length all operate during the first loading, and in the second loading no other source operates until the previous stress level is exceeded. This hypothesis, however, assumes that there is no rearrangement of dislocations during unloading, a situation more likely to happen in the materials that Agarwal tested, where the tendency for the dislocations to move back is small. It is hypothesized here that the dislocations that move back on unloading can move forward on reloading thus giving emission on second loading. This emission on second loading cannot be expected to be high as in the first loading.

The absence of a Kaiser effect in the fcc alloys can perhaps be explained on the basis of a model proposed by Makin[20]. He postulates that locks are formed during unloading and that these locks are broken on subsequent loading. His evidence for this is the reappearance of a yield point phenomenon on a second application of a load to a single crystal tensile specimen of 99.99% copper. The yield drop is directly proportional to the decrease in stress during unloading.

Since there are fewer slip systems to operate, the chances of Lomer-Cottrell locks forming in copper-7.9% aluminum alloy is decreased though it cannot be completely ruled out. Instead, it can be assumed that the dislocations in the active slip planes can move back and forth and that the ease of their motion depends on the nature of the friction stresses. While unloading, the dislocations are acted upon by the back-stresses. They move a certain distance, and then stop when they encounter an obstacle. The back-stresses cannot be relieved except by thermal means. The back-stress builds up until it is sufficient to cause dislocations to shear through the barriers. This planar motion of dislocations can take place back and forth depending on the direction of the effective stress.

5.6 99.95% Magnesium

It has been hypothesized above that if slip is confined to primary planes there is a greater likelihood of dislocations moving back and forth. If this were true, hcp metals, with slip confined to basal planes, should show a more pronounced effect.

99.95% magnesium samples were rolled to 1/8 in. thick and annealed. Fig. 13 shows the emission response. The amplitude of the emission bursts, load as well as unload, observed in this material were larger than in any other material tested during this investigation. The unload emission counts, as well as the emission on reloading, were found to be highest in magnesium of all materials tested. The absence of the Kaiser effect is easily explained by the fact that slip is confined to basal planes, especially at low stresses. The maximum applied stress did not exceed 5000 psi in the acoustic tests. Because the critical resolved shear stress for basal slip is 1/20 to 1/100 of that for pyramidal or prismatic slip, basal slip accounts for most of the deformation. Kelly and Hosford[4]

obtained stress-strain curves for magnesium of comparable purity for single crystals, textured polycrystalline materials, and polycrystalline materials with randomly oriented grains. The orientation of the specimens used in this investigation is comparable to the orientation designated as ZR in their work. It is reported that basal slip is more favorable in a large percentage of the grains in this orientation. The twinning mode is not predominant, especially in the stress range employed in the acoustic tests. The strain due to twinning is estimated to be less than 10% of the strain to which the specimens were subjected.

5.7 70-30 Brass

Annealed 70-30 brass specimens show considerable unload emission as seen in Fig. 19. The stacking fault energy of 70-30 brass is reported as 10 ergs/cm^2.[21] 70-30 brass exhibits mostly planar slip with a few dislocation dipoles. The large load emission and the absence of the Kaiser effect are consistent with the above hypothesis for unload emission response.

5.8 The Dependence of the Unload Emission on the Magnitude of the Bauschinger Effect.

It is of interest to compare the dependence of the unload emission on the amount of strain for several fcc materials. Fig. 19 showed a plot of strain vs unload emission and Fig. 16 a plot of $\frac{\sigma}{\sigma_{0.005}}$ vs ε, where $\sigma_{0.005}$ is the stress to which the specimen is subjected for a strain of 0.005 in./in, and ε is the strain during loading or unloading at a stress σ. The data are all for annealed material. It can be seen from Fig. 19 and Table V that as the stacking fault energy decreases in fcc metals, the unload emission increases for the same plastic strain. The way the Bauschinger strain is computed can be understood from Fig. 15.

TABLE V

STACKING FAULT ENERGY, BAUSCHINGER EFFECT AND UNLOAD EMISSION IN SEVERAL ANNEALED MATERIALS

Material	Crystal Structure	Stacking Fault Energy, erfs/cm^2	Bauschinger Strain, micro in/in*	Unload Emission, Counts#
99.99% aluminum	fcc	200	100	340
6061 aluminum alloy	fcc	117	480	610
2024 aluminum alloy	fcc	-	510	580
70-30 brass	fcc	10-12	1150	2400
Cu-7.9% aluminum alloy	fcc	4	1210	4700
99.95% magnesium	hcp		3000	12400

* Bauschinger strain was measured at a compressive stress which was 50% of the tensile stress needed to produce a strain of 0.005 in/in.

Unload emission counts were recorded for a cumulative plastic strain of 0.0001 in/in.

The Bauschinger strain values are tabulated in Table V. A correlation between the Bauschinger strain, stacking fault energy and unload emission counts can be noted by comparing Table V, Figs. 16, and 19. The copper-7.9% aluminum alloy shows the largest unload emission counts and the largest Bauschinger strain. 99.99% aluminum exhibits the least Bauschinger strain and also the lowest unload emission.

6.0 Conclusions

The following conclusions can be drawn on the basis of the experimental results and the discussion that have been presented.

1. There is a good correlation between the unload emission and the Bauschinger effect. Materials that exhibit large unload emission show a large Bauschinger effect.

2. The unload emission depends on the grain size of the specimen. In a large grain-sized sample, there are more strain pulses of amplitude above the threshold level of the measuring system because of large glide distances.

3. Materials that exhibit large unload emission do not show a Kaiser effect, i.e. they do show acoustic emission on repeated loading. It is likely that as long as the dislocations are confined to move in primary slip planes they can move back and forth during unloading and repeated loading. Planar glide materials such as a copper-7.9% aluminum alloy behave in this manner.

A plausible possible explanation for the acoustic emission behavior of materials during unloading is as follows. Unload emission is the result of reverse plastic deformation. However, dislocations must be available in the primary slip planes to cause reverse plastic deformation. Cross-slip reduces the availability of the dislocations in the primary planes to move back. Since the tendency for cross-slipping is more in materials with high stacking-fault energies, materials such as 99.99% aluminum give low acoustic emission during unloading. One the same basis, a planar glide material, such as a copper-7.9% aluminum bronze, and a 70-30 brass show considerable unload emission because they have a low

stacking-fault energy. For the same plastic strain, the emission from copper-7.9% aluminum alloy is 5 to 6 times that of 99.99% aluminum.

BIBLIOGRAPHY

1. Mitchell, L.D., "An Investigation of the Correlation of Acoustic Emission Phenomena and the Scatter in the Fatigue Data, "Ph.D. Thesis, The University of Michigan, (October 1965).

2. Feltner, C.E., and Laird, C., "Cyclic Stress-Strain Response of FCC Metals and Alloys- I., Phenomenological Experiments," Acta Met., Vol. 15, p. 1621, (October 1967).

3. Feltner, C.E., and Laird, C., "Cyclic Stress-Strain Response of FCC Metals and Alloys- II, Dislocation Structures and Mechanisms, "Acta Met., Vol. 15, p. 1633, (October 1967).

4. Kelly, E.W., and W.F. Hosford, Jr., "Deformation of Characteristics of Textured Magnesium." Trans. of the Metal. Soc. of AIME, Vol. 242, p. 654, (April 1968).

5. Young, Jr., F.W., "Elastic-plastic Transition in Copper Crystals as Determined by an Etch Pit Technique," Appl. Phys., Vol. 32, p. 1815, (1961).

6. Koppenaal, T.J., "Microstraining in a-Cu-Al Single Crystals," Acta Met., Vol. 11, p. 537, (June 1963).

7. Cottrell, A.H., "Dislocations and Plastic Deformation of Crystals," Oxford University Press, p. 112, (1965).

8. Nabarro, F.R.N., "Some recent developments in Rheology," British Rheology Club, London, (1950).

9. Kulhmann, D., "On Theory of Plastic Deformation, "Proc. Phy. Soc., (London), Vol. A 64, p. 140, (1951).

10. Deak, G.I., "A Study of the Causes of Bauschinger Effect," Doctoral Thesis, M.I.T., (January 1962).

11. Mott, N.F., "Imperfections in Nearly Perfect Crystals," W. Schockley, Ed., John Wiley and Sons, New York, (1952).

12. Seeger, A., and Tauble, H., Z. Metall., Vol. 51, p. 435.

13. Turnbull, J.A., "Comment on Dislocation Climb and Determination of Stacking Fault Energies in Aluminum and Aluminum-1% Magnesium Alloys," J. App. Phys. Vol. 38, p. 4075, (1967)

14. Seeger, A., "Dislocations and Mechanical Properties of Crystals," John Wiley and Sons, New York, (1957)

15. Segal, R.L., and Partridge, P.G., "Dislocation Arrangements in Aluminum Deformed in Tension or by Fatigue," Phil. Mag., Vol. 4, p. 912, (August 1959).

BIBLIOGRAPHY (CONT'D)

16. Thomas, G., and Nutting, J., "The Plastic Deformation of Aged Aluminum Alloys," Inst. Metals, Vol. 86, p. 7, (1958).

17. Abel, A., and Ham, R.K., "The Cyclic Behavior of Crystals of Aluminum 4wt% Copper - I, The Bauschinger Effect." Acta Met., Vol. 14, p. 1493, (November 1966).

18. Thomas, G., and Washburn, J., "Electron Microscopy and the Strength of Crystals," Interscience, New York and London (1963).

19. Agarwal, A.B.L., Frederick, J.R., and Felbeck, D.K., "Acoustic Emission from Unstable Dislocation Sources in 2024 Aluminum During Plastic Microstraining." (to be published in Trans. AIME).

20. Makin, M.J., "Unloading Effects on Plastic Properties of Copper Single Crystals," Phil Mag. Vol. 3, p. 287, (March 1958).

21. Whelan, M.J., Proc. Roy. Soc., Vol. A249, p. 114.

REPORT DISTRIBUTION LIST

Dr. George Martin
North American Rockwell Corp.
Los Angeles Division
International Airport
Los Angeles, California 90009

Mr. Phil Crimmins
Aerojet-General Corp.
Sacramento, California 95813

Dr. J. R. Frederick
University of Michigan
Dept. of Mechanical Engineering
2046 East Engineering
Ann Arbor, Michigan 48105

Professor R. H. Chambers
Dept. of Physics
Engineering Experiment Station
University of Arizona
Tucson, Arizona 85721

Mr. Darrell James
Dept. of Metallurgy
College of Engineering
University of Denver
University Park
Denver, Colorado 80210

Mr. Eugene Roffman
Frankford Arsenal
Fire Control Laboratories
Philadelphia, Pennsylvania 19137

Mr. Solomon Goldspiel
U.S. Naval Applied Science Laboratory
Flushing & Washington Avenues
Brooklyn, New York 11251

Mr. Otto Gericke
Test and Evaluation Methods
Army Material Command
Army Materials & Mechanics Research Center
Watertown, Massachusetts 02172

Lt. Col. Louis Klinker, U.S. Army
Office of Chief of Research & Development
Materials Science & Technology Branch
Highland Building
3045 Columbia Pike
Arlington, Virginia 22204

Mr. Howard Criscuolo
Naval Ordnance Library
Radiation Physics Division (code 223)
White Oak
Silver Spring, Maryland 20910

Mr. Stephen D. Hart
Naval Research Laboratory
Mechanics Division
Washington, D.C. 20390

Mr. F. S. Williams
Aero Materials Dept.
Naval Air Development Center
Warminston, Pennsylvania 18974

Dr. A. S. Tetelman, Head
Materials Division
College of Engineering
University of California
Los Angeles, California 90024

Dr. L. W. Orr
Department of Electrical Engineering
University of Michigan
Ann Arbor, Michigan 48105

Professor Emmett N. Leith
Dept. of Electrical Engineering
University of Michigan
Ann Arbor, Michigan 48105

J. L. Kreuzer
Optical Group
Perkin-Elmer
Norwalk, Connecticut 06850

D. D. Skinner
Fellow Engineer
Westinghouse Electric Corp.
Research Laboratories
Pittsburgh, Pennsylvania 15235

Dr. Volker Weiss
Assoc. Chairman
Dept. of Chemical Engineering
& Metallurgy
Syracuse University
Syracuse, New York 13210

Robert C. McMasters
Nondestructive Testing Research Lab.
Dept. of Welding Engineering
The Ohio State University
Columbus, Ohio 43210

Professor Lawrence Mann, Jr.
Dept. of Mechanical, Aerospace, and
Industrial Engineering
Louisiana State University
Baton Rouge, Louisiana 70803

Howard A. Johnson
The Boeing Company
Space Division, Aerospace Group
Kent Facility
P.O. Box 3868
Seattle, Washington 98124

C. Gerald Gardner
Southwest Research Institute
8500 Culebra Road
San Antonio, Texas 78206

Mr. Carlton H. Hastings
Chief, NDT Evaluation
AVCO Corp., Space Systems Div.
Lowell Industrial Park
Lowell, Massachusetts 01851

Mr. David Driscoll
U. S. Army Materials & Mechanics
Research Center
Watertown, Massachusetts 02172

Dr. R. C. Gause
Materials Division
Marshall Space Flight Center
Huntsville, Alabama 35800

AFML/MAMN
Attn: Lt. James W. Bohlen
Wright-Patterson AFB, Ohio 45433

Defense Documentation Center DDC
Cameron Station
Alexandria, Virginia 22314

Director of Advanced Research
Projects Agency
Washington, D.C. 20301

The Institute for Defense Analysis
400 Army-Navy Drive
Arlington, Virginia 22202

The Nondestructive Testing
Information Service
Watertown Arsenal
Watertown, Massachusetts 02172

Pravin G. Bhuta, Manager
Applied Mechanics Laboratory
Systems Group of TRW Inc.
One Space Park
Redondo Beach, California 90278

Allen Green
Aerojet-General Corporation
Materials Integrity Group
Dept. 0729, Bldg. 2931
Sacramento, California 95813

T. Theodore Anderson
Argonne National Laboratory
Reactor Engineering Division
D308
9700 S. Cass Avenue
Argonne, Illinois 60439

Phil Hutton & D. C. Worlton
Battelle-Northwest
P.O. Box 999
Richland, Washington 99352

Robert Moss
Boeing Scientific Research Lab.
1-8000
MS 01-14
Box 3981
Seattle, Washington 98124

Charles Musser
The Boeing Company
Saturn Booster Branch
Org. 5-172
MS LE-62
Box 29100
New Orleans, Louisiana 70129

Harvey L. Balderston
The Boeing Company
Space Division, Kent Facility
P.O. Box 3868
Seattle, Washington 98124
Attn: Orgn. 2-5022
Mail Stop

Thomas F. Drouillard
Dow Chemical Company
Rocky Flats Division
P.O. Box 888
Golden, Colorado 80401

R. E. Ringsmuth
Jet Propulsion Laboratory
California Institute of
Technology
4800 Oak Grove Drive
Pasadena, California 91103

Dwight Parry
Phillips Petroleum
P.O. Box 2067
Idaho Falls, Idaho 83401

Brad Schofield
Teledyne Materials Research
303 Bear Hill Road
Waltham, Massachusetts 02154

Hal Dunegan
University of California
Lawrence Radiation Laboratory
P.O. Box 808
Livermore, California 94550

C. D. Bailey
Lockheed-Georgia Company
Materials Development Laboratory
Department 72-14
Marietta, Georgia 30060

R. F. Saxe
North Carolina State University
Nuclear Engineering Department
P.O. Box 5636
Raleigh, North Carolina 27607

A. W. Porter
Government of Canada
Forest Products Laboratory
6620 N. W. Marine Drive
Vancouver 8, British Columbia
Canada

John G. Sessler
Materials Science
Syracuse University Research Corp.
Merrill Lane
Syracuse, New York 13210

L. J. Chockie
General Electric Company
175 Curtner Avenue
San Jose, California 95125

Lawrence Radiation Laboratory
Attn: Tech. Information Dept. L-3
P.O. Box 808
Livermore, California 94550

James Bryant
Office Chief of R&D
Attn: Cropes
3045 Columbia Pike,
Arlington, Virginia 22204